

1 Asynchronous Carbon Sink Saturation in African and Amazonian Tropical Forests

2

3 Authors

4 Wannès Hubau^{1,2,3*}, Simon L. Lewis^{1,4*}, Oliver L. Phillips¹, Kofi Affum-Baffoe⁵, Hans Beeckman², Aida
5 Cuní-Sánchez^{4,6}, Armandu K. Daniels⁷, Corneille E.N. Ewango^{8,9,10}, Sophie Fauset^{11,1}, Jacques M. Mukinzi
6 ^{8,12,13}, Douglas Sheil^{14,15,16}, Bonaventure Sonké¹⁷, Martin J.P. Sullivan^{1,18}, Terry C.H. Sunderland^{16,19}, Hermann
7 Taedoumg^{17,20}, Sean C. Thomas²¹, Lee J.T. White^{22,23,24}, Katharine A. Abernethy^{24,23}, Stephen Adu-Bredu²⁵,
8 Christian A. Amani^{26,16}, Timothy R. Baker¹, Lindsay F. Banin²⁷, Fidèle Baya^{28,29}, Serge K. Begne^{17,1}, Amy C.
9 Bennett¹, Fabrice Benedet^{30,31}, Robert Bitariho¹⁵, Yannick E. Bocko³², Pascal Boeckx³³, Patrick Boundja^{34,16,35},
10 Roel J.W. Brienen¹, Terry Brncic³⁴, Eric Chezeaux³⁶, George B. Chuyong³⁷, Connie J. Clark³⁸, Murray
11 Collins^{39,40}, James A. Comiskey^{41,42}, David A. Coomes⁴³, Greta C. Dargie¹, Thales de Haulleville², Marie Noel
12 Djuikouo K.³⁷, Jean-Louis Doucet⁴⁴, Adriane Esquivel-Muelbert^{1,45}, Ted R. Feldpausch⁴⁶, Alusine Fofanah⁴⁷,
13 Ernest G. Foli²⁵, Martin Gilpin¹, Emanuel Gloor¹, Christelle Gonmadje⁴⁸, Sylvie Gourlet-Fleury^{30,31}, Jefferson
14 S. Hall⁴⁹, Alan C. Hamilton⁵⁰, David J. Harris⁵¹, Terese B. Hart^{52,53}, Mireille B.N. Hockemba³⁴, Annette
15 Hladik⁵⁴, Suspense A. Ifo⁵⁵, Kathryn J. Jeffery²⁴, Tommaso Jucker⁵⁶, Emmanuel Kasongo Yakusu^{10,3,2}, Elizabeth
16 Kearsley^{57,2}, David Kenfack^{49,58}, Alexander Koch^{4,59}, Miguel E. Leal⁶⁰, Aurora Levesley¹, Jeremy A.
17 Lindsell^{61,62}, Janvier Lisingo⁶³, Gabriela Lopez-Gonzalez¹, Jon C. Lovett^{1,64}, Jean-Remy Makana⁶³, Yadvinder
18 Malhi⁶⁵, Andrew R. Marshall^{6,66,67}, Jim Martin⁶⁸, Emanuel H. Martin^{58,69}, Faustin M. Mbayu¹⁰, Vincent P.
19 Medjibe^{70,71,38}, Vianet Mihindou^{71,22}, Edward T.A. Mitchard³⁹, Sam Moore⁶⁵, Pantaleo K.T. Munishi⁷², Natacha
20 Nssi Bengone²², Lucas Ojo⁷³, Fidèle Evouna Ondo⁷¹, Kelvin Peh^{74,75}, Georgia C. Pickavance¹, Axel D.
21 Poulsen⁵¹, John R. Poulsen³⁸, Lan Qie^{1,76}, Jan Reitsma⁷⁷, Francesco Rovero^{78,79}, Michael D. Swaine⁸⁰, Joey
22 Talbot¹, James Taplin⁸¹, David M. Taylor⁸², Duncan W. Thomas⁸³, Benjamin Toirambe^{84,2}, John Tshibamba
23 Mukendi^{2,10,85}, Darlington Tuagben⁷, Peter M. Umunay^{86,87}, Geertje M.F. Van Der Heijden⁸⁸, Hans Verbeeck⁵⁷,
24 Jason Vleminckx^{89,90}, Simon Willcock⁹¹, Hannsjoerg Woell⁹², John T. Woods⁹³, Lise Zemagho¹⁷

25

26 *Contributed equally

27

28 **Author affiliations**

- 29 1. University of Leeds, School of Geography, Leeds, UK
- 30 2. Royal Museum for Central Africa, Service of Wood Biology, Tervuren, Belgium
- 31 3. Ghent University, Department of Environment, Laboratory of Wood Technology (Woodlab),
32 Ghent, Belgium
- 33 4. University College London, Department of Geography, London, UK
- 34 5. Forestry Commission of Ghana, Mensuration Unit, Kumasi, Ghana
- 35 6. University of York, Department of Environment and Geography, York, UK
- 36 7. Forestry Development Authority of the Government of Liberia (FDA), Monrovia, Liberia
- 37 8. Wildlife Conservation Society, DR Congo Programme, Kinshasa, Democratic Republic of
38 Congo
- 39 9. Centre de Formation et de Recherche en Conservation Forestiere (CEFRECOF), Epulu,
40 Democratic Republic of Congo
- 41 10. Université de Kisangani, Faculté de Gestion de Ressources Naturelles Renouvelables,
42 Kisangani, Democratic Republic of Congo
- 43 11. University of Plymouth, School of Geography, Earth and Environmental Sciences, Plymouth,
44 UK
- 45 12. Salonga National Park, Kinshasa, Democratic Republic of Congo
- 46 13. World Wide Fund for Nature, Gland, Switzerland
- 47 14. Norwegian University of Life Sciences, Faculty of Environmental Sciences and Natural
48 Resource Management, Ås, Norway
- 49 15. Mbarara University of Science and Technology (MUST), The Institute of Tropical Forest
50 Conservation (ITFC) , Mbarara, Uganda
- 51 16. Center for International Forestry Research (CIFOR), Bogor, Indonesia

- 52 17. University of Yaounde I, Plant Systematic and Ecology Laboratory, Higher Teachers' Training
53 College, Yaounde, Cameroon
- 54 18. Manchester Metropolitan University, Department of Natural Sciences, Manchester, UK
- 55 19. University of British Columbia, Faculty of Forestry, Vancouver, Canada
- 56 20. Biodiversity International, Yaounde, Cameroon
- 57 21. University of Toronto, Faculty of Forestry, Toronto, Canada
- 58 22. Ministry of Forests, Seas, Environment and Climate, Libreville, Gabon
- 59 23. Institut de Recherche en Ecologie Tropicale, Libreville, Gabon
- 60 24. University of Stirling, Biological and Environmental Sciences, Stirling, UK
- 61 25. Forestry Research Institute of Ghana (FORIG), Kumasi, Ghana
- 62 26. Université Officielle de Bukavu, Bukavu, Democratic Republic of Congo
- 63 27. Centre for Ecology and Hydrology, Penicuik, UK
- 64 28. Ministère des Eaux, Forêts, Chasse et Pêche (MEFCP), Bangui, Central African Republic
- 65 29. Institut Centrafricain de Recherche Agronomique (ICRA), Bangui, Central African Republic
- 66 30. Centre de coopération International en Recherche Agronomique pour le Développement
67 (CIRAD), Forêts et Sociétés (F&S), Montpellier, France
- 68 31. Université de Montpellier, Forêts et Sociétés (F&S), Montpellier, France
- 69 32. Université Marien Ngouabi, Faculté des Sciences et Techniques, Laboratoire de Botanique et
70 Ecologie, Brazzaville, Republic of Congo
- 71 33. Ghent University, Isotope Bioscience Laboratory-ISOFYS, Gent, Belgium
- 72 34. Wildlife Conservation Society, Congo Programme, Brazzaville, Republic of Congo
- 73 35. Resources and Synergies Development (R&SD), Singapore, Singapore
- 74 36. Rougier-Gabon, Libreville, Gabon
- 75 37. University of Buea, Faculty of Science, Department of Botany and Plant Physiology, Buea,
76 Cameroon

- 77 38. Duke University, Nicholas School of the Environment, Durham, NC, USA
- 78 39. University of Edinburgh, School of GeoSciences, Edinburgh, UK
- 79 40. Grantham Research Institute on Climate Change and the Environment, London, UK, London,
80 UK
- 81 41. National Park Service, Inventory & Monitoring Program, Fredericksburg, VA, USA
- 82 42. Smithsonian Institution, Washington, DC, USA
- 83 43. University of Cambridge, Department of Plant Sciences, Cambridge, UK
- 84 44. University of Liège, Forest Resources Management, Gembloux Agro-Bio Tech, Liège,
85 Belgium
- 86 45. University of Birmingham, School of Geography, Earth and Environmental Sciences,
87 Birmingham, UK
- 88 46. University of Exeter, Geography, College of Life and Environmental Sciences, Exeter, UK
- 89 47. The Gola Rainforest National Park, Kenema, Sierra Leone
- 90 48. National Herbarium, Yaounde, Cameroon
- 91 49. Smithsonian Tropical Research Institute, Forest Global Earth Observatory (ForestGEO),
92 Washington, DC, USA
- 93 50. Kunming Institute of Botany, Kunming, China
- 94 51. Royal Botanic Garden Edinburgh, Edinburgh, UK
- 95 52. Lukuru Wildlife Research Foundation, Kinshasa, Democratic Republic of Congo
- 96 53. Yale Peabody Museum of Natural History, Division of Vertebrate Zoology, New Haven, CT,
97 USA
- 98 54. Muséum National d'Histoire Naturel, Département Hommes, natures, sociétés, Paris, France
- 99 55. Université Marien Ngouabi, École Normale Supérieure (ENS), Département des Sciences et
100 Vie de la Terre, Laboratoire de Géomatique et d'Ecologie Tropicale Appliquée, Brazzaville,
101 Republic of Congo

- 102 56. University of Bristol, School of Biological Sciences, Bristol, UK
- 103 57. Ghent University, Department of Environment, Computational & Applied Vegetation Ecology
104 (Cavelab), Ghent, Belgium
- 105 58. Tropical Ecology, Assessment and Monitoring (TEAM) Network, Arlington, VA, USA
- 106 59. University of Hong Kong, Department of Earth Sciences, Hong Kong, Hong Kong SAR
- 107 60. Wildlife Conservation Society, Uganda Programme, Kampala, Uganda
- 108 61. A Rocha International, Cambridge, UK
- 109 62. The Royal Society for the Protection of Birds, Centre of Conservation Science, Sandy, UK
- 110 63. Université de Kisangani, Faculté des Sciences, Laboratoire d'écologie et aménagement
111 forestier, Kisangani, Democratic Republic of Congo
- 112 64. Royal Botanic Gardens, Kew, UK
- 113 65. University of Oxford, Environmental Change Institute, School of Geography and the
114 Environment, Oxford, UK
- 115 66. University of the Sunshine Coast, Tropical Forests and People Research Centre, Sippy Downs,
116 Australia
- 117 67. Flamingo Land Ltd, Kirby Misperton, UK
- 118 68. Fleming College, Peterborough, Canada
- 119 69. Udzungwa Ecological Monitoring Centre, Mang'ula, Tanzania
- 120 70. Commission of Central African Forests (COMIFAC), Yaounde, Cameroon
- 121 71. Agence Nationale des Parcs Nationaux, Libreville, Gabon
- 122 72. Sokoine University of Agriculture, Morogoro, Tanzania
- 123 73. University of Abeokuta, Abeokuta, Nigeria
- 124 74. University of Southampton, School of Biological Sciences, Southampton, UK
- 125 75. University of Cambridge, Department of Zoology, Conservation Science Group, Cambridge,
126 UK

- 127 76. University of Lincoln, School of Life Sciences, Lincoln, UK
- 128 77. Bureau Waardenburg, Culemborg, The Netherlands
- 129 78. University of Florence, Department of Biology, Florence, Italy
- 130 79. MUSE - Museo delle Scienze, Tropical Biodiversity Section , Trento, Italy
- 131 80. University of Aberdeen, Department of Plant & Soil Science, School of Biological Sciences,
- 132 Aberdeen, UK
- 133 81. UK Research & Innovation, Innovate UK, London, UK
- 134 82. National University of Singapore, Department of Geography, Singapore, Singapore
- 135 83. Washington State University, Biology Department, Vancouver, WA, USA
- 136 84. Ministère de l'Environnement et Développement Durable, Kinshasa, Democratic Republic of
- 137 Congo
- 138 85. Université de Mbuji-Mayi, Faculté des Sciences Appliquées, Mbuji-Mayi, Democratic Republic
- 139 of Congo
- 140 86. Yale University, Yale School of Forestry & Environmental Studies, New Haven, CT, USA
- 141 87. Wildlife Conservation Society, New York, NY, USA
- 142 88. University of Nottingham, School of Geography, Nottingham, UK
- 143 89. Florida International University, International Center for Tropical Botany, Department of
- 144 Biological Sciences, Florida, FL, USA
- 145 90. Université Libre de Bruxelles, Faculté des Sciences, Service d'Évolution Biologique et
- 146 écologie, Brussels, Belgium
- 147 91. University of Bangor, School of Natural Sciences, Bangor, UK
- 148 92. Sommersbergseestrasse, Bad Aussee, Austria
- 149 93. University of Liberia, W.R.T College of Agriculture and Forestry, Monrovia, Liberia

150

151

152 **Summary**

153

154 **Structurally intact tropical forests sequestered ~50% of global terrestrial carbon uptake over**
155 **the 1990s and early 2000s, removing ~15% of anthropogenic CO₂ emissions¹⁻³. Climate-driven**
156 **vegetation models typically predict that this tropical forest ‘carbon sink’ will continue for**
157 **decades^{4,5}. Here, we assess trends in the carbon sink using 244 structurally intact African**
158 **tropical forests spanning 11 countries, we compare them with 321 published plots from**
159 **Amazonia and investigate the underlying drivers of the trends. The carbon sink in live**
160 **aboveground biomass in intact African tropical forests has been stable for the three decades to**
161 **2015, at 0.66 Mg C ha⁻¹ yr⁻¹ (95% CI:0.53-0.79), in contrast to the long-term decline in**
162 **Amazonian forests⁶. Thus, the carbon sink responses of Earth’s two largest expanses of tropical**
163 **forest have diverged. The difference is largely driven by carbon losses from tree mortality, with**
164 **no detectable multi-decadal trend in Africa and a long-term increase in Amazonia. Both**
165 **continents show increasing tree growth, consistent with the expected net effect of rising**
166 **atmospheric CO₂ and air temperature⁷⁻⁹. Despite the past stability of the African carbon sink,**
167 **our data suggest a post-2010 increase in carbon losses, delayed compared to Amazonia,**
168 **indicating asynchronous carbon sink saturation on the two continents. A statistical model**
169 **including CO₂, temperature, drought and forest dynamics accounts for the observed trends and**
170 **indicates a long-term future decline in the African sink, while the Amazonian sink continues to**
171 **rapidly weaken. Overall, the uptake of carbon into Earth’s intact tropical forests peaked in the**
172 **1990s. Given that the global terrestrial carbon sink is increasing in size, observations indicating**
173 **greater recent carbon uptake into the Northern hemisphere landmass¹⁰ reinforce our conclusion**
174 **that the intact tropical forest carbon sink has already saturated. This tropical forest sink**
175 **saturation and ongoing decline has consequences for policies to stabilise Earth’s climate.**

176 **Main text**

177

178 Tropical forests account for approximately one-third of Earth's terrestrial Gross Primary Productivity
179 and one-half of Earth's carbon stored in terrestrial vegetation¹¹. Thus, small biome-wide changes in
180 tree growth and mortality can have global impacts, either buffering or exacerbating the increase in
181 atmospheric CO₂. Models^{2,4,5,7,12}, ground-based observations¹³⁻¹⁵, airborne atmospheric CO₂
182 measurements^{3,16}, inferences from remotely sensed data¹⁷, and synthetic approaches^{3,8,18} each suggest
183 that, after accounting for land-use change, remaining structurally intact tropical forests (i.e. not
184 impacted by direct anthropogenic impacts such as logging) are increasing in carbon stocks. This
185 structurally intact tropical forest carbon sink is estimated at ~1.2 Pg C yr⁻¹ over 1990-2007 using scaled
186 inventory plot measurements¹. Yet, despite its policy relevance, changes in this key carbon sink remain
187 highly uncertain^{19,20}.

188

189 Globally the terrestrial carbon sink is increasing^{2,7,8,21}. Between 1990 and 2017 the land surface
190 sequestered ~30% of all anthropogenic carbon dioxide emissions^{1,21}. Rising CO₂ concentrations are
191 thought to have boosted photosynthesis more than rising air temperatures have enhanced respiration,
192 resulting in an increasing global terrestrial carbon sink^{2,4,7,8,21}. Yet, for Amazonia, recent results from
193 repeated censuses of intact forest inventory plots show a progressive two-decade decline in sink
194 strength primarily due to an increase of carbon losses from tree mortality⁶. It is unclear if this simply
195 reflects region-specific drought impacts^{22,23}, or potentially chronic pan-tropical impacts of either heat-
196 related tree mortality^{24,25}, or internal forest dynamics resulting from past increases in carbon gains
197 leaving the system²⁶. A more recent deceleration of the rate of increase in carbon gains from tree
198 growth is also contributing to the declining Amazon sink⁶. Again, it is not known if this is a result of
199 either pan-tropical CO₂ fertilisation saturation, or rising air temperatures, or is merely a regional
200 drought impact. To address these uncertainties, we (i) analyze an unprecedented long-term inventory

201 dataset from Africa, (ii) pool the new African and existing Amazonian records to investigate the
202 putative environmental drivers of changes in the tropical forest carbon sink, and (iii) project its likely
203 future evolution.

204

205 We collected, compiled and analysed data from structurally intact old-growth forests from the African
206 Tropical Rainforest Observation Network²⁷ (217 plots) and other sources (27 plots) spanning the
207 period 1968 to 2015 (Extended Data Figure 1; Supplementary Table 1). In each plot (mean size, 1.1
208 ha), all trees ≥ 100 mm in stem diameter were identified, mapped and measured at least twice using
209 standardised methods (135,625 trees monitored). Live biomass carbon stocks were estimated for each
210 census date, with carbon gains and losses calculated for each interval (Extended Data Figure 2).

211

212 **Continental Carbon Sink Trends**

213 We detect no long-term trend in the per unit area African tropical forest carbon sink over three decades
214 to 2015 (Figure 1). The aboveground live biomass sink averaged $0.66 \text{ Mg C ha}^{-1} \text{ yr}^{-1}$ (95% CI: 0.53-
215 0.79; $n=244$) and was significantly greater than zero for every year since 1990 (Figure 1). While very
216 similar to past reports ($0.63 \text{ Mg C ha}^{-1} \text{ yr}^{-1}$)¹³, this first estimate of the temporal trend in Africa contrasts
217 with the declining Amazonian trend⁶ (Figure 1). A linear mixed effect model shows a significant
218 difference in the slopes of the sink trends for the two continents over the common time window (pooled
219 data from both continents, common time window, 1983-2011.5; $p=0.017$). Thus, the per unit area sink
220 strength of the two largest expanses of tropical forest on Earth diverged in the 1990s and 2000s.

221

222 The proximal cause of the divergent sink patterns is a significant increase in carbon losses (from tree
223 mortality, i.e. the loss of carbon from the live biomass pool) in Amazonian forests, with no detectable
224 trend over three decades in African forests (Figure 1). A linear mixed effects model using pooled data
225 shows a significant difference in slopes of carbon losses between the two continents over the common

226 1983-2011.5 time window ($p=0.027$). Long-term trends in carbon gains (from tree growth and newly
227 recruited trees) on both continents show significant increases (Figure 1), and we could detect no
228 difference in slopes between the continents ($p=0.348$; carbon gains from tree growth alone also show
229 no continental difference in long-term trends, $p=0.322$). However, an assessment of how underlying
230 environmental drivers affect carbon gains and losses is needed to understand the ultimate causes of the
231 divergent sink patterns.

232

233 **Understanding the Carbon Sink Trends**

234 We first investigate environmental drivers exhibiting long-term change that impact theory-driven
235 models of photosynthesis and respiration: atmospheric CO₂ concentration, surface air temperature, and
236 water availability. A linear mixed effects model of carbon gains, with censuses nested within plots,
237 and pooling the new African and published Amazonian data, shows a significant positive relationship
238 with CO₂, and significant negative relationships with mean annual temperature (MAT) and drought
239 (measured as the Maximum Climatological Water Deficit, MCWD¹⁴; Figure 2; Extended Data Table
240 1). These results are consistent with a positive CO₂ fertilisation effect, and negative effects of higher
241 temperatures and drought on tree growth, consistent with temperature-dependent increases in
242 autotrophic respiration, and temperature- and drought-dependent reductions in carbon assimilation. By
243 contrast, the equivalent model for carbon losses (i.e. tree mortality) shows no significant relationships
244 with CO₂, MAT or MCWD (Figure 2; Extended Data Table 1).

245

246 We further investigate the responses of carbon gains and losses (for which the above analysis has no
247 explanatory power) by expanding our potential explanatory variables to additionally include the
248 change in environmental conditions (CO₂-change, MAT-change, MCWD-change, see Extended Data
249 Figure 3 for calculation details), and two attributes of forests that may influence their response to the
250 same environmental change: plot mean wood density (which in old-growth forests correlates with

251 below-ground resource availability^{28,29}), and the plot carbon residence time (which measures how long
252 fixed carbon remains in the system, hence dictates when past increases in carbon gains leave the system
253 as elevated carbon losses³⁰).

254

255 The minimum adequate carbon gain model using our expanded explanatory variables (best ranked
256 model using multimodel inference) has a positive relationship with CO₂-change, and negative
257 relationships with MAT, MAT-change, MCWD, and wood density (Table 2; model-average results
258 are similar, see Methods and Supplementary Tables 2-4). The retention of both MAT and MAT-change
259 suggests that higher temperatures correspond to lower tree growth, and that trees only partially
260 acclimate to recently rising temperatures, which further reduces growth, consistent with warming
261 experiments³¹ and observations⁹. The inclusion of higher wood density, and it being related to lower
262 carbon gains (Extended Data Figure 4), alongside no temporal trends in wood density (Extended Data
263 Figure 5), suggests that old-growth forests with denser-wooded tree communities typically have fewer
264 available below-ground resources, or such patterns may also emerge from disturbance regimes lacking
265 large-scale exogenous events, consistent with prior studies^{26,28,32}.

266

267 The minimum adequate carbon gain model using our expanded explanatory variables also highlights
268 continental differences. Between 2000 and 2015 African forest carbon gains increased by 3.1%
269 compared with a 0.1% decline in Amazonia over the same interval (Table 2). In Africa, from 2000 to
270 2015, the increase was composed of a 3.7% increase from CO₂-change, partially offset by increasing
271 droughts depleting gains by 0.5%, and only a slight decline in gains of 0.1% resulting from temperature
272 increases (Table 2), because the rate of temperature change (MAT-change) decelerated over this time
273 window (Extended Data Figure 5). For Amazonia, the same 3.7% increase due to CO₂-change was
274 seen, while increasing droughts—and these forests' greater sensitivity to drought—reduced gains by
275 2.7% (five times the impact in Africa), and temperature increases at the same rate as in the past (i.e.

276 MAT-change is zero) further reduced gains by 1.1% (ten times the impact in Africa), leaving a net
277 change in gains slightly below zero (Table 2). Thus, the recent stalling of carbon gain increases in
278 Amazonia⁶ is a response to drought and temperature and not due to an unexpected saturation of CO₂
279 fertilisation. Overall, the larger modelled increase in gains in Africa relative to Amazonia appear to be
280 driven by slower warming, fewer or less extreme droughts, lower forest sensitivity to droughts, and
281 overall lower temperatures (African forests are on average ~1.1°C cooler than Amazonian forests, as
282 they typically grow at ~200 m higher elevation). Other continental differences may also be influencing
283 the results, including higher nitrogen deposition in African tropical forests due to the seasonal burning
284 of nearby savannas³³ and biogeographic history resulting in differing contemporary species pools and
285 resulting functional attributes^{34,35}.

286

287 The minimum adequate carbon loss model using our expanded explanatory variables shows higher
288 losses with CO₂-change and MAT-change, and lower losses with MCWD and the carbon residence
289 time (CRT; Table 2). Thus, changes in carbon losses appear to be largely a function of carbon gains.
290 First, the greater losses in forests with shorter CRT conform to a ‘high-gain high-loss’ forest dynamics
291 pattern²⁶. Second, wetter plots have a longer growing season and so have higher gains and
292 correspondingly higher losses, explaining the negative relationship with MCWD. Third, as increasing
293 CO₂ levels result in additional carbon gains, after some time these additional past gains leave the
294 system resulting in greater carbon losses, explaining the positive relationship with CO₂-change.
295 Finally, in addition to these relationships with carbon gains, the inclusion of MAT-change (p<0.001)
296 indicates heat- or vapour pressure deficit-induced tree mortality²⁴. Overall, our results imply that
297 chronic long-term environmental change factors, temperature and CO₂, rather than simply the direct
298 effects of drought, underlie longer-term trends in tropical forest tree mortality, although other changes
299 such as rising liana infestation rates seen in Amazonia^{36,37} cannot be excluded.

300

301 The minimum adequate carbon loss model using our expanded explanatory variables replicates the
302 continental trends (Figure 3). The overall lower loss rates in Africa reflect their longer CRT (69 yrs,
303 95% CI, 66-72), compared with Amazonian forests (56 yrs, 95% CI, 54-59) while over the 2000-2015
304 window the much smaller increase in loss rates in Africa compared to Amazonia results from a slower
305 increase in warming and a stable CRT in Africa compared to continued warming at previous rates and
306 a shortening CRT in Amazonian forests (Extended Data Figure 5). Furthermore, given that losses
307 appear to lag behind gains they should relate to the long-term CRT of plots. This is what we find: the
308 longer the CRT the smaller the increase in carbon losses, with no increase in losses for plots with CRT
309 ≥ 77 years (Extended Data Figure 6). Consequently, due to the typically longer residence times of
310 African forests, increasing losses in Africa ought to appear 10-15 years after the increase in Amazon
311 losses began (*c.*1995). Strikingly, in Africa the most intensely monitored plots suggest that losses
312 began increasing from *c.*2010 (Extended Data Figure 7), and plots with shorter CRT are driving the
313 increase (Extended Data Figure 8). Thus, a mortality-dominated African carbon sink decline appears
314 to have begun very recently.

315

316 **Future of the Tropical Forest Carbon Sink**

317 Our carbon gain and loss models (Table 2) can be used to make a tentative estimate of the future size
318 of the per unit area intact forest carbon sink (Figure 3). Extrapolations of the changes in the predictor
319 variables from 1983-2015 forward to 2040 (Extended Data Figure 5) show declines in the sink on both
320 continents (Figure 3). By 2030 the carbon sink in aboveground live biomass in intact African tropical
321 forest is predicted to decline by 14% from the measured 2010-15 mean, to $0.57 \text{ Mg C ha}^{-1} \text{ yr}^{-1}$ (2σ
322 range, 0.16-0.96; Figure 3). The Amazon sink continues to decline, reaching zero in 2035 (2σ range,
323 2011-2089; Figure 3). Our estimated sink strength on both continents in the 2020s and 2030s is
324 sensitive to future CO_2 emissions pathways (CO_2 -change)³⁸, resulting temperature increase (MAT,
325 MAT-change) and hydrological changes (MCWD), plus changes in forest dynamics (CRT), but the

326 sink is always lower than levels seen in the 2000s (see Methods and Supplementary Table 5). Thus,
327 the carbon sink strength of the world's two most extensive tropical forests have now saturated, albeit
328 asynchronously.

329

330 **Scaling Results to the Pan-tropics**

331 Scaling our estimated mean sink strength by forest area for each continent signifies that Earth recently
332 passed the point of peak carbon sequestration into intact tropical forests (Table 1). The continental sink
333 in Amazonia peaked in the 1990s, followed by a decline, driven by sink strength peaking in the 1990s
334 and a continued decline in forest area (Table 1). In Africa the per unit area sink strength peaked later
335 in the 2000-2010 period, but the continental African sink peaked in the 1990s, due to the decline in
336 forest area in the 2000s outpacing the small per unit area increase in sink strength. Including the modest
337 uptake in the much smaller area of intact Asian tropical forest indicates that total pan-tropical carbon
338 uptake peaked in the 1990s (Table 1). From peak pan-tropical intact forest uptake of 1.26 Pg C yr⁻¹ in
339 the 1990s, we project a continued decline reaching just 0.29 Pg C yr⁻¹ in the 2030s (multi-decade
340 decline of ~0.24 Pg C yr⁻¹ decade⁻¹), driven by (i) reduced mean pan-tropical sink strength decline of
341 0.1 Mg C ha⁻¹ yr⁻¹ decade⁻¹ and (ii) ongoing forest area losses of ~13.5 million ha yr⁻¹ (see Extended
342 Data Table 2 for forest area details). Critically, climate-driven vegetation model simulations have not
343 predicted that peak net carbon uptake into intact tropical forests has already been passed^{2,4,5}.

344

345 **Discussion**

346 Our method of scaling to arrive at a pan-tropical sink estimate – in common with other studies using
347 similar datasets^{1,6,13} – is limited. Yet, pervasive net carbon uptake is expected given that we find a
348 strong and ongoing CO₂ fertilisation effect. Using our CO₂ response in Table 2, we find an increase in
349 aboveground carbon stocks of 10.8±3.7 Mg C ha⁻¹ 100 ppm⁻¹ CO₂, or 6.5±2.2% (±SE; using an area-
350 weighted pan-tropical mean aboveground C stock of 165 Mg C ha⁻¹), comparable to the 5.0±1.2%

351 increase in tropical forest C stocks 100 ppm⁻¹ CO₂ derived from a recent synthesis of CO₂ fertilisation
352 experiments, despite a lack of data from mature tropical forests³⁹. Our result is within the range of
353 climate-driven vegetation models^{2,7}, although it is greater than a number of recently-published models
354 that include potential nutrient constraints, reported as 5.9±4.7 Mg C ha⁻¹ 100 ppm⁻¹ CO₂ (Ref.⁴⁰). We
355 find that the CO₂ fertilisation uptake is currently only partially offset by the negative impacts of
356 similarly widespread rising air temperatures (-2.0±0.4 Mg C ha⁻¹ °C⁻¹, from Table 2), consistent with
357 models⁷, limited experiments³¹ and independent observations⁹, plus negative responses to drought^{41,42}.
358 Long-term and extensive increases in satellite-derived greenness in tropical regions not experiencing
359 major changes in land-use management^{17,43}, particularly in central Africa in the past decade⁴⁴, indicate
360 increases in tropical forest net primary productivity, providing further evidence that the sink is a
361 widespread phenomenon⁴⁴.

362

363 Nonetheless, our analyses show that this pervasive tropical forest sink in live biomass is in long-term
364 decline, first saturating in Amazonia, and more recently followed by African forests, explaining the
365 prior Africa-Amazon carbon sink divergence as part of a longer-term pattern of asynchronous
366 saturation and decline. From an atmospheric perspective the full impacts of the contribution to the
367 saturation of the sink from slowing carbon gains are experienced immediately, but the contribution
368 from rising carbon losses is delayed because dead trees do not decompose instantaneously.
369 Decomposition of this dead tree mass is ~50% in 4 yrs, and ~85% in 10 yrs, thus rising carbon losses
370 result in delayed carbon additions to the atmosphere⁴⁵. Hence, from an atmospheric perspective the
371 intact tropical forest biomass carbon sink likely peaked a few years later than our plot data indicate
372 and the full impacts are not yet realised. The pan-tropical carbon sink in live biomass reduced by 0.27
373 Pg C yr⁻¹ between the 1990s and 2000s (Table 1), but accounting for dead wood decomposition⁴⁵
374 shows a smaller 0.17 Pg C yr⁻¹ reduction from an atmospheric perspective (see Methods).

375

376 Given that the global terrestrial carbon sink is increasing, a weakening intact tropical forest sink
377 implies that the extra-tropical carbon sink has increased over the past two decades. Independent
378 observations of inter-hemispheric atmospheric CO₂ concentration indicates that carbon uptake into the
379 Northern hemisphere landmass has increased at a greater rate than the global terrestrial carbon sink
380 since the 1990s, with a further disproportionate increase in the 2000s¹⁰. The inter-hemispheric analysis
381 suggests a weakening of the tropical forest sink by ~0.2 Pg C yr⁻¹ between the 1990s and 2000s¹⁰,
382 which is similar to the 0.17 Pg C yr⁻¹ weakening over the same time period that we find. This reinforces
383 our conclusion that the intact tropical forest carbon sink has already saturated.

384

385 In summary, our results indicate that while intact tropical forests remain major stores of carbon and
386 are key centres of biodiversity¹¹, their ability to sequester additional carbon is waning. In the 1990s
387 intact forests removed 17% of anthropogenic CO₂ emissions. This has declined to 6% in the 2010s,
388 because the pan-tropical weighted average per unit area sink strength declined by 33%, forest area
389 decreased by 19%, and CO₂ emissions increased by 46%. Although tropical forests are more
390 immediately threatened by deforestation⁴⁶ and degradation⁴⁷, and the future carbon balance will also
391 depend on secondary forest dynamics⁴⁸ and forest restoration plans⁴⁹, our analyses show that they are
392 also impacted by atmospheric chemistry and climatic changes. Given that the intact tropical forest
393 carbon sink is set to end sooner than even the most pessimistic climate-driven vegetation models
394 predict^{4,5}, our analyses suggest that climate change impacts in the tropics may become more severe
395 than predicted. Furthermore, the carbon balance of intact tropical forests will only stabilise once CO₂
396 concentrations and the climate stabilises.

397

398 Continued on-the-ground monitoring of the world's remaining intact tropical forests will be required
399 to test our prediction that the intact tropical forest carbon sink will continue to decline. Such direct
400 ground-based measurements also provide a constraint on estimating the size and location of the

401 terrestrial carbon sink. In addition, our conclusion that tree mortality and internal forest dynamics are
402 important controls on the future of the tropical forest carbon sink, may assist in improving the
403 vegetation components of future Earth System Models⁵⁰ and contribute to reducing terrestrial carbon
404 cycle feedback uncertainty^{19,20}. Our findings also have policy implications. At the country-level: given
405 intact tropical forests are a carbon sink, but the size is changing, national greenhouse gas reporting will
406 require careful forest monitoring. At the international-level: given tropical forests are likely to
407 sequester less carbon in the future than Earth System Models predict, an earlier date to reach net zero
408 anthropogenic greenhouse gas emissions will be required to meet any given commitment to limit the
409 global heating of Earth.

410

411 **References**

412

- 413 1 Pan, Y. *et al.* A Large and Persistent Carbon Sink in the World's Forests. *Science* **333**, 988-
414 993, doi:10.1126/science.1201609 (2011).
- 415 2 Sitch, S. *et al.* Recent trends and drivers of regional sources and sinks of carbon dioxide.
416 *Biogeosciences* **12**, 653-679, doi:10.5194/bg-12-653-2015 (2015).
- 417 3 Gaubert, B. *et al.* Global atmospheric CO₂ inverse models converging on neutral tropical land
418 exchange, but disagreeing on fossil fuel and atmospheric growth rate. *Biogeosciences* **16**, 117-
419 134, doi:10.5194/bg-16-117-2019 (2019).
- 420 4 Huntingford, C. *et al.* Simulated resilience of tropical rainforests to CO₂-induced climate
421 change. *Nature Geoscience* **6**, 268-273, doi:10.1038/ngeo1741 (2013).
- 422 5 Mercado, L. M. *et al.* Large sensitivity in land carbon storage due to geographical and temporal
423 variation in the thermal response of photosynthetic capacity. *New Phytologist* **218**, 1462-1477,
424 doi:doi:10.1111/nph.15100 (2018).
- 425 6 Brienen, R. J. W. *et al.* Long-term decline of the Amazon carbon sink. *Nature* **519**, 344-348,
426 doi:10.1038/nature14283 (2015).

- 427 7 Piao, S. *et al.* Evaluation of terrestrial carbon cycle models for their response to climate
428 variability and to CO₂ trends. *Global Change Biology* **19**, 2117-2132, doi:10.1111/gcb.12187
429 (2013).
- 430 8 Schimel, D., Stephens, B. B. & Fisher, J. B. Effect of increasing CO₂ on the terrestrial carbon
431 cycle. *Proceedings of the National Academy of Sciences* **112**, 436-441,
432 doi:10.1073/pnas.1407302112 (2015).
- 433 9 Anderegg, W. R. L. *et al.* Tropical nighttime warming as a dominant driver of variability in the
434 terrestrial carbon sink. *Proceedings of the National Academy of Sciences* **112**, 15591-15596,
435 doi:10.1073/pnas.1521479112 (2015).
- 436 10 Ciais, P. *et al.* Five decades of northern land carbon uptake revealed by the interhemispheric
437 CO₂ gradient. *Nature*, doi:10.1038/s41586-019-1078-6 (2019).
- 438 11 Lewis, S. L., Edwards, D. P. & Galbraith, D. Increasing human dominance of tropical forests.
439 *Science* **349**, 827-832, doi:10.1126/science.aaa9932 (2015).
- 440 12 Pugh, T. A. M. *et al.* Role of forest regrowth in global carbon sink dynamics. *Proceedings of*
441 *the National Academy of Sciences* **116**, 4382-4387, doi:10.1073/pnas.1810512116 (2019).
- 442 13 Lewis, S. L. *et al.* Increasing carbon storage in intact African tropical forests. *Nature* **457**,
443 1003-1006, doi:10.1038/nature07771 (2009).
- 444 14 Phillips, O. L. *et al.* Drought sensitivity of the Amazon rainforest. *Science* **323**, 1344-1347,
445 doi:10.1126/science.1164033 (2009).
- 446 15 Qie, L. *et al.* Long-term carbon sink in Borneo's forests halted by drought and vulnerable to
447 edge effects. *Nature Communications* **8**, 1966, doi:10.1038/s41467-017-01997-0 (2017).
- 448 16 Gatti, L. V. *et al.* Drought sensitivity of Amazonian carbon balance revealed by atmospheric
449 measurements. *Nature* **506**, 76-80, doi:10.1038/nature12957 (2014).
- 450 17 Nemani, R. R. *et al.* Climate-driven increases in global terrestrial net primary production from
451 1982 to 1999. *Science* **300**, 1560-1563 (2003).

- 452 18 Keenan, T. F. *et al.* Recent pause in the growth rate of atmospheric CO₂ due to enhanced
453 terrestrial carbon uptake. *Nature Communications* **7**, 13428, doi:10.1038/ncomms13428
454 (2016).
- 455 19 Booth, B. B. B. *et al.* High sensitivity of future global warming to land carbon cycle processes.
456 *Environmental Research Letters* **7**, 024002 (2012).
- 457 20 Lombardozzi, D. L., Bonan, G. B., Smith, N. G., Dukes, J. S. & Fisher, R. A. Temperature
458 acclimation of photosynthesis and respiration: A key uncertainty in the carbon cycle-climate
459 feedback. *Geophysical Research Letters* **42**, 8624-8631, doi:doi:10.1002/2015GL065934
460 (2015).
- 461 21 Le Quéré, C. *et al.* Global Carbon Budget 2018. *Earth Syst. Sci. Data* **10**, 2141-2194,
462 doi:10.5194/essd-10-2141-2018 (2018).
- 463 22 Lewis, S. L., Brando, P. M., Phillips, O. L., van der Heijden, G. M. F. & Nepstad, D. The 2010
464 Amazon Drought. *Science* **331**, 554 (2011).
- 465 23 Feldpausch, T. R. *et al.* Amazon forest response to repeated droughts. *Global Biogeochemical*
466 *Cycles* **30**, 964-982, doi:doi:10.1002/2015GB005133 (2016).
- 467 24 McDowell, N. *et al.* Drivers and mechanisms of tree mortality in moist tropical forests. *New*
468 *Phytologist* **219**, 851-869, doi:doi:10.1111/nph.15027 (2018).
- 469 25 Aleixo, I. *et al.* Amazonian rainforest tree mortality driven by climate and functional traits.
470 *Nature Climate Change* **9**, 384-388, doi:10.1038/s41558-019-0458-0 (2019).
- 471 26 Lewis, S. L. *et al.* Concerted changes in tropical forest structure and dynamics: evidence from
472 50 South American long-term plots. *Philosophical Transactions of the Royal Society of London*
473 *Series B-Biological Sciences* **359**, 421-436 (2004).
- 474 27 Lewis, S. L. *et al.* Above-ground biomass and structure of 260 African tropical forests.
475 *Philosophical Transactions of the Royal Society B: Biological Sciences* **368**, 20120295-
476 20120295, doi:10.1098/rstb.2012.0295 (2013).

- 477 28 Quesada, C. A. *et al.* Basin-wide variations in Amazon forest structure and function are
478 mediated by both soils and climate. *Biogeosciences* **9**, 2203-2246, doi:10.5194/bg-9-2203-
479 2012 (2012).
- 480 29 Malhi, Y. *et al.* The above-ground coarse wood productivity of 104 Neotropical forest plots.
481 *Global Change Biology* **10**, 563-591 (2004).
- 482 30 Galbraith, D. *et al.* Residence times of woody biomass in tropical forests. *Plant Ecology &*
483 *Diversity* **6**, 139-157, doi:10.1080/17550874.2013.770578 (2013).
- 484 31 Reich, P. B. *et al.* Boreal and temperate trees show strong acclimation of respiration to
485 warming. *Nature* **531**, 633-636, doi:10.1038/nature17142 (2016).
- 486 32 ter Steege, H. *et al.* Continental-scale patterns of canopy tree composition and function across
487 Amazonia. *Nature* **443**, 444-447 (2006).
- 488 33 Bauters, M. *et al.* High fire-derived nitrogen deposition on central African forests. *Proceedings*
489 *Of The National Academy Of Sciences Of The United States Of America* **115**, 549-554,
490 doi:10.1073/pnas.1714597115 (2018).
- 491 34 Parmentier, I. *et al.* The odd man out? Might climate explain the lower tree alpha-diversity of
492 African rain forests relative to Amazonian rain forests? *Journal of Ecology* **95**, 1058-1071
493 (2007).
- 494 35 Slik, J. W. F. *et al.* Phylogenetic classification of the world's tropical forests. *Proceedings of*
495 *the National Academy of Sciences* **115**, 1837-1842, doi:10.1073/pnas.1714977115 (2018).
- 496 36 Phillips, O. L. *et al.* Increasing dominance of large lianas in Amazonian forests. *Nature* **418**,
497 770-774 (2002).
- 498 37 Schnitzer, S. A. & Bongers, F. Increasing liana abundance and biomass in tropical forests:
499 emerging patterns and putative mechanisms. *Ecology Letters* **14**, 397-406, doi:10.1111/j.1461-
500 0248.2011.01590.x (2011).

- 501 38 Meinshausen, M. *et al.* The RCP greenhouse gas concentrations and their extensions from 1765
502 to 2300. *Climatic Change* **109**, 213-241, doi:10.1007/s10584-011-0156-z (2011).
- 503 39 Terrer, C. *et al.* Nitrogen and phosphorus constrain the CO₂ fertilization of global plant
504 biomass. *Nature Climate Change*, doi:10.1038/s41558-019-0545-2 (2019).
- 505 40 Fleischer, K. *et al.* Amazon forest response to CO₂ fertilization dependent on plant phosphorus
506 acquisition. *Nature Geoscience* **12**, 736-741, doi:10.1038/s41561-019-0404-9 (2019).
- 507 41 Jiang, Y. *et al.* Widespread increase of boreal summer dry season length over the Congo
508 rainforest. *Nature Climate Change* **9**, 617-622, doi:10.1038/s41558-019-0512-y (2019).
- 509 42 Gloor, M. *et al.* Recent Amazon climate as background for possible ongoing and future changes
510 of Amazon humid forests. *Global Biogeochemical Cycles* **29**, 1384-1399,
511 doi:10.1002/2014gb005080 (2015).
- 512 43 Kolby Smith, W. *et al.* Large divergence of satellite and Earth system model estimates of global
513 terrestrial CO₂ fertilization. *Nature Climate Change* **6**, 306, doi:10.1038/nclimate2879 (2015).
- 514 44 Chen, C. *et al.* China and India lead in greening of the world through land-use management.
515 *Nature Sustainability* **2**, 122-129, doi:10.1038/s41893-019-0220-7 (2019).
- 516 45 Chambers, J. Q., Higuchi, N., Schimel, J. P., Ferreira, L. V. & Melack, J. M. Decomposition
517 and carbon cycling of dead trees in tropical forests of the central Amazon. *Oecologia* **122**, 380-
518 388 (2000).
- 519 46 Hansen, M. C. *et al.* High-Resolution Global Maps of 21st-Century Forest Cover Change.
520 *Science* **342**, 850-853, doi:10.1126/science.1244693 (2013).
- 521 47 Pearson, T. R. H., Brown, S., Murray, L. & Sidman, G. Greenhouse gas emissions from tropical
522 forest degradation: an underestimated source. *Carbon Balance and Management* **12**, 3,
523 doi:10.1186/s13021-017-0072-2 (2017).
- 524 48 Schwartz, N. B., Uriarte, M., DeFries, R., Gutierrez-Velez, V. H. & Pinedo-Vasquez, M. A.
525 Land-use dynamics influence estimates of carbon sequestration potential in tropical second-

526 growth forest. *Environmental Research Letters* **12**, 074023, doi:10.1088/1748-9326/aa708b
527 (2017).

528 49 Lewis, S. L., Wheeler, C. E., Mitchard, E. T. A. & Koch, A. Regenerate natural forests to store
529 carbon. *Nature* **568**, 25-28 (2019).

530 50 Yu, K. *et al.* Pervasive decreases in living vegetation carbon turnover time across forest climate
531 zones. *Proceedings of the National Academy of Sciences*, 201821387,
532 doi:10.1073/pnas.1821387116 (2019).

533

534 **Acknowledgements**

535 This paper is a product of the African Tropical Rainforest Observatory Network (AfriTRON), curated
536 at ForestPlots.net. AfriTRON has been supported by numerous people and grants since its inception.

537 We sincerely thank the people of the many villages and local communities who welcomed our field
538 teams and without whose support this work would not have been possible: Sierra Leone (Barrie, Gaura,
539 Koya, Makpele, Malema, Nomo, Tunkia, Gola Rainforest National Park), Liberia (Garley town, River
540 Gbeh, Glaro Freetown), Ghana (Nkwanta, Asenanyo, Bonsa, Agona, Boekrom, Dadieso, Enchi,
541 Dabiasem, Mangowase, Draw, Fure, Esuboni, Okumaninin, Kadeand Asamankese, Tinte Bepo,
542 Tonton), Nigeria (Oban), Gabon (Ekobakoba, Mikongo, Babilone, Makokou, Leke/Moyabi Rougier
543 Forestry Concession, Ivindo National Park, Lope National Park, Ipassa station, Kingele station,
544 Tchimbele, Mondah, Ivindo, Ebe, Ekouk, Oveng, Sette Cama, Waka National Park), Cameroon
545 (Campo, Nazareth, Lomié, Djomédjo, Alat-Makay, Somolomo, Deng Deng, Ejagham forest reserve,
546 Eyumojok, Mbakaou, Myere, Nguti, Bejange, Kekpane, Basho, Mendhi, Matene, Mboh, Takamanda,
547 Obonyi, Ngoïla), Democratic Republic of Congo (Yoko, Yangambi, Epulu, Monkoto), Republic of
548 Congo (Bomassa, Ekolongouma, Bolembe, Makao, Mbeli, Kabo, Niangui, Ngubu, Goualaki,
549 Essimbi), and many others.

550

551 We thank the hundreds of field assistants whose expertise and enthusiasm is indispensable to
552 successful fieldwork: Menge Elvis Abang, Usaw Philip Achui, Francis Addai, Eyelechon Julius
553 Agbachon, Jess Agnaka , Archaley John Akaza, Gabarie Alaman, Gregoire Alaman, Abor Enow
554 Alexander, Kate Allen, Mobembe Amalphi, Danny Amandus, Jean Andju, Lazare Angassike
555 Limbanga, Samuel Asamoah, Takem Martin Ashu, Moses Ashu, Joel Asse, Bangubaare Augustine,
556 Henry Badjoko, Mayanga Balimu, Juste Baviogui-Baviogui, Solomon Benteh, Akuemo Bertrand,
557 Akwo Bettus, Albert Bias, Andre Bikoula, Alain Bimba, Prince Bissiemou, Mensah Boateng, Etshu
558 Bonyenga, Mopero Bosiko Ekaya, Gael Bouka, Juvenal Boussengui, Didier Bowaka Ngomo, Charles
559 Chalange, Sylvester Chenikan, Jonathan Dabo, Emmanuel Dadize, Takyi Degraft, Joachim Dibakou,
560 Jean-Thoussaint Dikangadissi, Pacôme Dimbonda, Edmond Dimoto, Carl Ditougou, Daniel Dorbor,
561 Morris Dorbor, Vincent Droissart, Kwaku Duah, Edward Ebe, Osong Jerome Eji, Ekama Bertrand
562 Ekamam, Jean-Robert Ekomindong, Essa Joseph Enow, Hiboux Entombo, Ebai Mengue Ernest,
563 Courageux Esola, Jules Essouma, Alaman Gabriel, Nteh Genesis, Bilfanim Gideon, Afedo Godwin,
564 Eric Grear, D. John Grear, Mokondo Ismael, Michel Iwango, Mongali Iyafo, Narcisse Kamdem,
565 Bondele Kibinda, Alidé Kidimbu, Exaldi Kimumbu, John Kintsieri, Cisquet Kiebou Opepa, Amani
566 Kitegile, Thérance Komo, Pokou Koué, Augustin Kouanga, Jean Jules Koumikaka, Innocent Liengola,
567 Elias Litonga, Lisa Louvouando, Ondo Luis, Noé Madingou Mady, Felicien Mahoula, Amani
568 Mahundu, Chris Axel Mandebet, Pougue Maurice, Karl Yannick Mayossa, Robert Mba Nkogue, Isa
569 David Mbe, Christian Mbina, Herve Mbona, Alain Mboni, Alain Mbouni, Paulin Menzo, Michael
570 Menge, Andah Michael, Alain Mindoumou, Joseph Minpsa, Jean Paul Mondjo, E. Mounoumoulossi,
571 Serge Mpouam, Tofile Msigala, John Msirikale, Samuel Mtoka, Ruben Mwakisoma, Daniel Ndong-
572 Nguema, Gilbert Ndoyame, Guy Ngongbo, Francois Ngowa, D. Nguema, Luwi Nguye, Raoul
573 Niangadouma, Yaw Nkrumah, Seya Nshimba, Marcel Nziengui Mboumba, Francis Nzogo Obiang,
574 Lucas Obi, Roland Obi, Eyong Louis Odjong, Félix Okon, Fabiane Oliveira, Alina Lawrence
575 Owemicho, Leandre Oyeni-Amoni, Abia Platini, Pierre Ploton, Simon Quausah, Elasi Ramazani,

576 Boscu Saïdou Jean, Lebienfalteur Sagang, Rosalind Salter, Adenani Seki, Deo Shirima, Murielle Simo,
577 Igor Singono, Agboloh Eugene Tabi, Tako Gilbert Tako, Nteh Gambisi Tambe, Toha Tcho, Andrew
578 Teah, Victor Tehtoe, Bright Joe Telephas, Marie Lesly Tonda, Angoni Tresor, Hamid Umenendo,
579 Raymond Votere, Cyrus K. Weah, Slonean Weah, Bart Wursten, Emmanuel Yalley, Donatien Zebaze,
580 Laurent Cerbonney, Emilien Dubiez, Hervé Moinecourt, François Lanckriet, Evina, Monazang,
581 Engonga, Soso Samai, Mohamed Swaray, Patrick Lamboi, Mohamed Sullay, Dennis Bannah, Ibrahim
582 Kanneh, Michael Kannah, Alhassan Kemokai, Joseph Kenneh, Morrison Lukulay.

583

584 For logistical and administrative support, we are indebted to international, national and local
585 institutions: the Forestry Department of the Government of Sierra Leone, the Conservation Society of
586 Sierra Leone, the Royal Society for the Protection of Birds (RSPB), The Gola Rainforest National
587 Park, the Forestry Development Authority of the Government of Liberia (FDA), the University of
588 Liberia, the Forestry Commission of Ghana (FC), the Forestry Research Institute of Ghana (FORIG),
589 University of Ibadan (Nigeria), the University of Abeokuta (Nigeria), the Ministère des Eaux, Forêts,
590 Chasse et Pêche (MEFCP, Bangui, République Centrafricaine), the Institut Centrafricain de Recherche
591 Agronomique (ICRA), The Service de Coopération et d'Actions Culturelles (SCAC/MAE), The
592 University of Bangui, the Société Centrafricaine de Déroulage (SCAD), the University of Yaounde I,
593 the National Herbarium of Yaounde, the University of Buea, Biodiversity International (Cameroon),
594 the Ministry of Forests, Seas, Environment and Climate (Gabon), the Agence Nationale des Parcs
595 Nationaux de Gabon (ANPN), Institut de Recherche en Ecologie Tropicale du Gabon, Rougier-Gabon,
596 the Marien Ngouabi University of Brazzaville, the Ministère des Eaux et Forêts (République du
597 Congo), the Ministère de la Recherche Scientifique et de l'Innovation Technologique (République du
598 Congo), the Nouabalé-Ndoki Foundation, WCS-Congo, Salonga National Park, The Centre de
599 Formation et de Recherche en Conservation Forestière (CEFRECOF, Epulu, D.R.Congo), the Institut
600 National pour l'Etude et la Recherche Agronomiques en R.D.Congo (INERA), the École Régionale

601 Postuniversitaire d'Aménagement et de Gestion intégrés des Forêts et Territoires tropicaux (ERAIFT
602 Kinshasa), WWF-D.R.Congo, WCS-D.R.Congo, the Université de Kisangani, Université Officielle de
603 Bukavu, Université de Mbuji-Mayi, le Ministère de l'Environnement et Développement Durable de la
604 R.D.C., the Lukuru Wildlife Research Foundation, Mbarara University of Science and Technology
605 (MUST), WCS-Uganda, the Uganda Forest Department, the Commission of Central African Forests
606 (COMIFAC), the Udzungwa Ecological Monitoring Centre (Tanzania) and the Sokoine University of
607 Agriculture (Tanzania).

608

609 Grants that have funded the AfriTRON network including data in this paper are: a NERC grant to
610 O.L.P., Y.M., and S.L.L. (NER/A/S/2000/01002), a Royal Society University Research Fellowship to
611 S.L.L., a NERC New Investigators Grant to S.L.L., a Philip Leverhulme Award to S.L.L., a European
612 Union FP7 grant to E.G. and S.L.L. (GEOCARBON; 283080), Valuing the Arc Leverhulme Program
613 Grant to Andrew Balmford and S.L.L., a European Research Council Advanced Grant to O.L.P. and
614 S.L.L. (T-FORCES; 291585; Tropical Forests in the Changing Earth System), a Natural Environment
615 Research Council (NERC) Consortium Grant to Jon Lloyd and S.L.L. (TROBIT; NE/D005590/), the
616 Gordon and Betty Moore Foundation to L.J.T.W. and S.L.L., the David and Lucile Packard Foundation
617 to L.J.T.W. and S.L.L., the Centre for International Forestry Research to T.S. and S.L.L. (CIFOR), and
618 Gabon's National Parks Agency (ANPN) to S.L.L. W.H. was funded by T-FORCES and the Brain
619 program of the Belgian Federal Government (BR/132/A1/AFRIFORD and
620 BR/143/A3/HERBAXYLAREDD grants to H.B.). O.L.P., S.L.L., M.J.P.S, A.E.-M., A.L., G.L.-G.,
621 G.P, and L.Q were supported by T-FORCES.

622

623 Additional African data were included from the consortium MEFCP-ICRA-CIRAD (Centre de
624 Coopération Internationale en Recherche Agronomique pour le Développement), the Tropical Ecology
625 Assessment and Monitoring Network (TEAM), and the Forest Global Earth Observatory Network

626 (ForestGEO; formerly the Center for Tropical Forest Science CTFS). The TEAM network is a
627 collaboration between Conservation International, the Missouri Botanical Garden, the Smithsonian
628 Institution and the Wildlife Conservation Society, and funded by the Gordon and Betty Moore
629 Foundation and other donors. The ForestGEO Network is a collaboration between the Smithsonian
630 Institution, other federal agencies of the United States, the Wildlife Conservation Society (WCS) and
631 the World Wide Fund for Nature (WWF), and funded by the U.S. National Science Foundation and
632 other donors.

633

634 The paper was made possible by the RAINFOR network in Amazonia, with multiple funding agencies
635 and hundreds of investigators working in Amazonia, acknowledged in Ref.⁶, providing comprehensive
636 published data and code and allowing onward analysis of their data, see Ref.⁶. Data from AfriTRON
637 and RAINFOR are stored and curated by ForestPlots.net, a long-term cyber-infrastructure initiative
638 hosted at the University of Leeds that unites permanent plot records and their contributing scientists
639 from the world's tropical forests. The development of ForestPlots.net and curation of most data
640 analysed here was funded by many sources, including grants to S.L.L. (Royal Society University
641 Research Fellowship, NERC New Investigators Award, NERC NE/P008755/1), O.L.P. (principally
642 from NERC NE/B503384/1, ERC AdG 291585 "T-FORCES", and Gordon and Betty Moore
643 Foundation #1656, "RAINFOR") and E.G. ("GEOCARBON", and NE/F005806/1 "AMAZONICA").
644 We acknowledge the contributions of the ForestPlots.net steering committee (T.R.B., A.L., S.L.L.,
645 O.L.P., L.Q., Euridice N. Honorio Coronado and Beatriz S. Marimon) to advising on database
646 development and management.

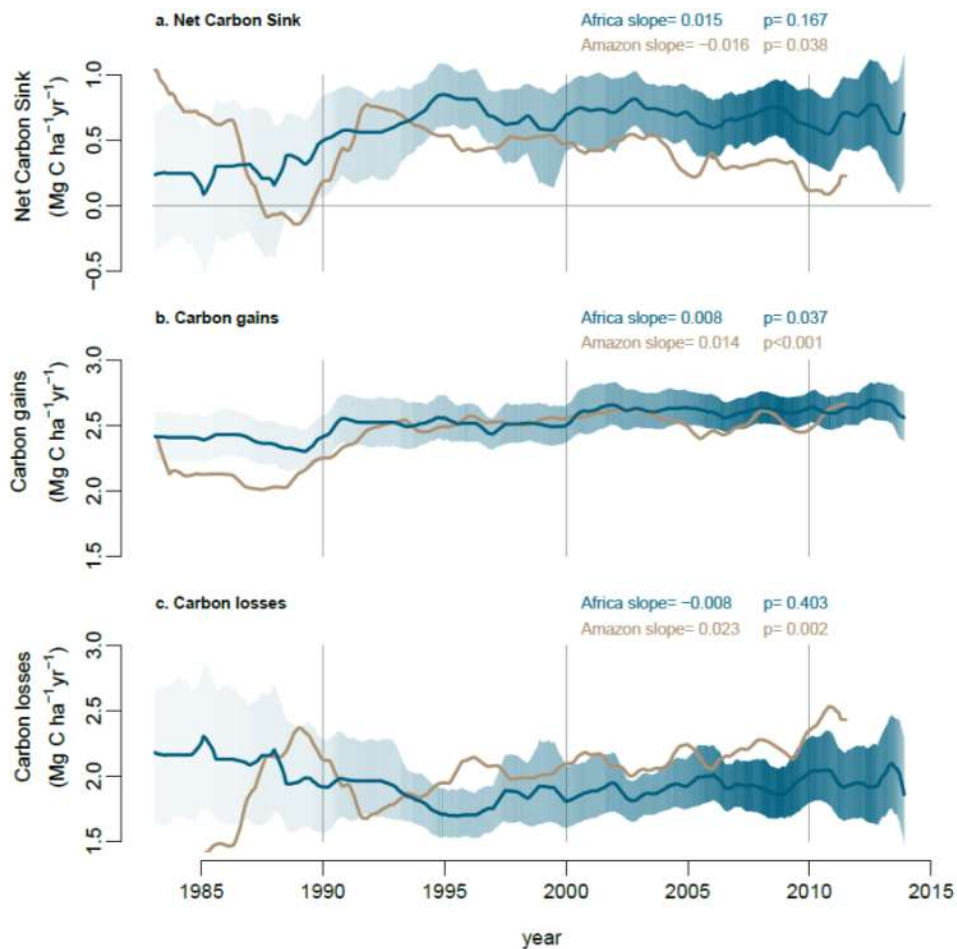
647

648 **Author Contributions**

649 S.L.L. conceived and managed the AfriTRON forest plot recensus programme, O.L.P., T.C.H.S,
650 L.J.T.W. and Y.M. contributed to its development. W.H., S.L.L., O.L.P., B.S. & M.J.P.S. developed

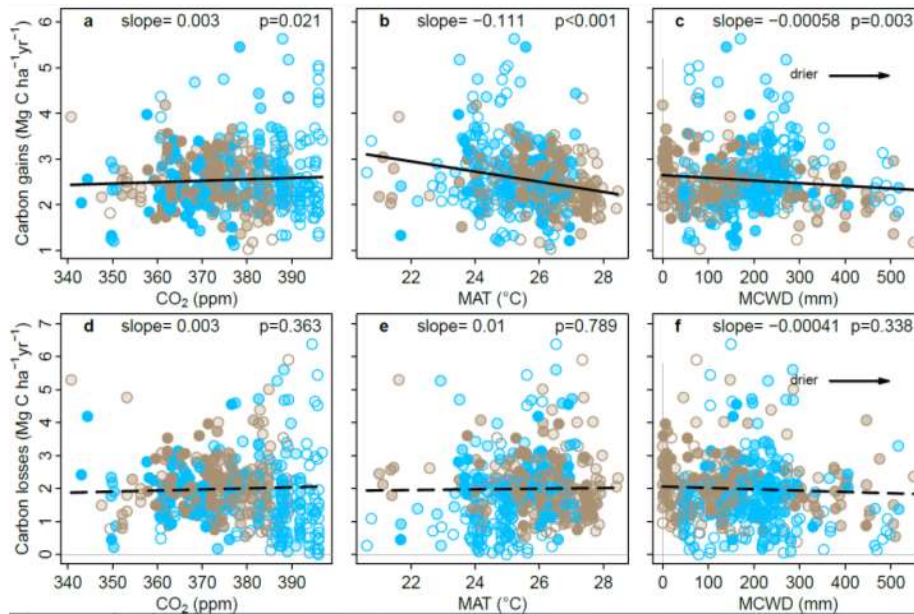
651 the study. W.H., S.L.L., O.L.P., K.A.-B., H.B., A.C.-S., C.E.N.E., S.F., D.S., B.S., T.C.H.S., S.C.T.,
652 K.A.A., S.A.-B., C.A.A., T.R.B., L.F.B., F.Ba., S.K.B., F.Be., R.B., Y.E.B., P.Boe., P.Bou., T.B., E.C.,
653 G.B.C., C.J.C., M.C., J.A.C., D.C., A.K.D., G.C.D., T.d.H., M.D.K., J.-L.D., T.R.F., A.F., E.G.F.,
654 M.G., C.G., S.G.-F., J.S.H., A.C.H., D.J.H., T.B.H., M.B.N.H., A.H., S.A.I., K.J.J., T.J., E.K.Y., E.K.,
655 D.K., M.E.L., J.A.L., J.L., J.C.L., J.-R.M., Y.M., A.R.M., J.M., E.H.M., F.M.M., V.P.M., V.M.,
656 E.T.A.M., S.M., J.M.M., P.K.T.M., N.N.B., L.O., F.E., K.P., A.D.P., J.R.P., L.Q., J.R., F.R., M.D.S.,
657 H.T., J.Tal., J.Tap., D.M.T., D.W.T., B.T., J.T.M., D.T., P.M.U., G.V.D.H., H.V., J.V., L.J.T.W., S.W.,
658 H.W., J.T.W. and L.Z. contributed data (larger field contributions by S.L.L, W.H., A.C.-S., B.S., H.T.,
659 A.K.D., C.E.N.E, J.M.M., K.A.-B. and S.F.). O.L.P., T.R.B., S.L.L. and G.L.-G. conceived and
660 managed forestplots.net; O.L.P., T.R.B., S.L.L., E.G., G.L.-G., G.C.P., A.L., R.J.W.B., T.R.F. and
661 M.J.P.S. developed it. W.H., M.J.P.S., S.L.L., O.L.P., R.J.W.B., A.L., G.L.-G., A.E.-M., A.K., E.G.,
662 T.R.B., A.C.B. and G.C.P. contributed analysis tools. W.H. and S.L.L. analysed the data (with
663 important contributions from M.J.P.S.). S.L.L. and W.H. wrote the paper. All co-authors read and
664 approved the manuscript (with important insights provided by O.L.P., S.F., R.J.W.B., E.G., H.B., D.S.,
665 M.J.P.S., S.G.-F., P.B., H.V. and S.C.T).

666



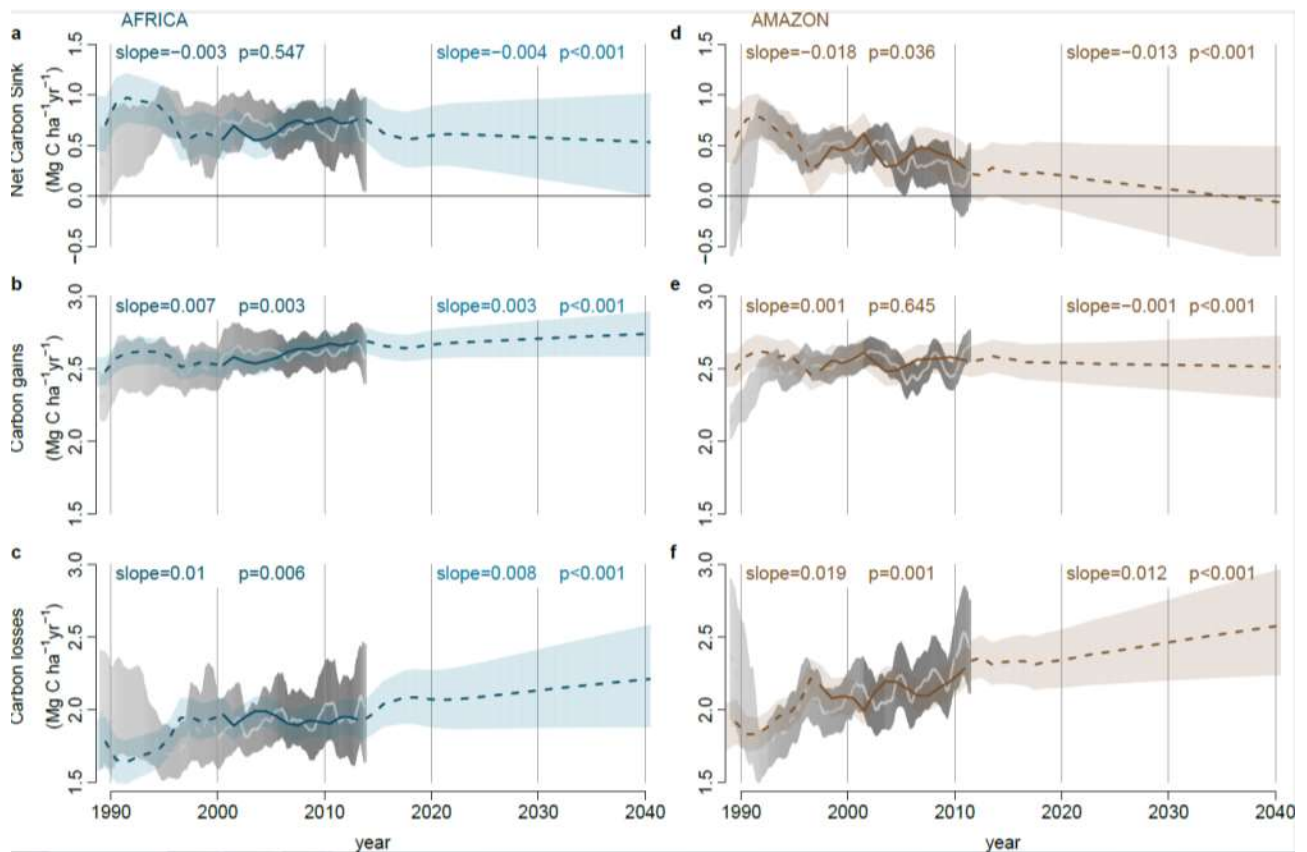
668

669 **Figure 1. Long-term carbon dynamics of structurally intact tropical forests in Africa (blue) and**
 670 **Amazonia (brown).** Trends in net aboveground live biomass carbon sink (a), carbon gains to the
 671 system from wood production (b), and carbon losses from the system from tree mortality (c), measured
 672 in 244 African inventory plots (blue lines) and contrasting published⁶ Amazonian inventory data
 673 (brown lines; 321 plots). Shading corresponds to the 95% CI, with less transparent shading indicating
 674 a greater number of plots monitored in that year (most transparent: minimum 25 plots monitored). The
 675 CI for the Amazonian dataset is omitted for clarity, but can be seen in Figure 3. Slopes and p-values
 676 are from linear mixed effects models (see Methods).



677

678 **Figure 2. Potential environmental drivers of carbon gains and losses in structurally intact old-**
679 **growth African and Amazonian tropical forests.** Aboveground carbon gains, from woody
680 production (a-c), and aboveground carbon losses, from tree mortality (d-f), presented as time-weighted
681 mean values for each plot, i.e. each census within a plot is weighted by its length, against the
682 corresponding values of atmospheric carbon dioxide concentration (CO₂), mean annual air temperature
683 (MAT) and drought (as Maximum Climatological Water Deficit, MCWD), for African (blue) and
684 Amazonian (brown) inventory plots. Each data point therefore represents an inventory plot, for visual
685 clarity, and the level of transparency represents the total monitoring length, with empty circles
686 corresponding to plots monitored for ≤ 5 years and solid circles for plots monitored for >20 years.
687 Solid lines show significant trends, dashed lines non-significant trends calculated using linear mixed
688 effect models with census intervals (n=1566) nested within plots (n=565), using an empirically derived
689 weighting based on interval length and plot area, on the untransformed pooled Africa and Amazon
690 dataset (see Methods). Slopes and p-values are from the same linear mixed effects models. Carbon loss
691 data and models are presented untransformed for comparison with carbon gains, but transformation is
692 needed to fit normality assumptions; linear mixed effects models on transformed carbon loss data does
693 not change the significance of the results, nor does including all three parameters and transformed data
694 in a model (see Extended Data Table 1).



695

696

697

698

699

700

701

702

703

704

705

706

707

708

Figure 3. Modelled past and future carbon dynamics of structurally intact tropical forests in Africa and Amazonia. Predictions of net aboveground live biomass carbon sink (a,d), carbon gains (b,e), and carbon losses (c,f), for African (left panels) and Amazonian (right panels) plot inventory networks, based on CO₂-change, Mean Annual Temperature, Mean Annual Temperature-change, drought (as Maximum Climatological Water Deficit), plot wood density, and plot carbon residence time, using observations in Africa until 2014 and Amazonia until 2011.5, and extrapolations of prior trends to 2040. Model predictions are in blue (Africa) and brown (Amazon), with solid lines spanning the window when $\geq 75\%$ of plots were monitored to show model consistency with the observed trends, and shading showing upper and lower confidence intervals accounting for uncertainties in the model (both fixed and random effects) and uncertainties in the predictor variables. Light grey lines and grey shading are the mean and 95% CI of the observations from the African and Amazonian plot networks.

Main Tables

709 **Table 1. Carbon sink in intact forests in Africa, Amazonia and the pan-tropics: 1980-2015 and**
710 **predictions to 2040.** Mean values in bold, future predictions in italics, uncertainty in parentheses, 95%
711 bootstrapped confidence intervals for 1980-2015, and 2σ for the predictions (2010-2040).

Period	No. plots		Per unit area aboveground live biomass C sink				Total C sink *		
			(Mg C ha ⁻¹ yr ⁻¹)				(Pg C yr ⁻¹)		
	Af. Am.	Africa	Amazon	Pan-tropics†	Africa	Amazon	Pan-tropics†		
1980-1990	45	73	0.33 (0.06-0.63)	0.35 (0.06-0.59)	0.35 (0.07-0.62)	0.28 (0.05-0.53)	0.49 (0.08-0.82)	0.87 (0.16-1.52)	
1990-2000	96	172	0.67 (0.43-0.89)	0.53 (0.42-0.65)	0.57 (0.39-0.74)	0.50 (0.32-0.66)	0.68 (0.54-0.83)	1.26 (0.88-1.63)	
2000-2010	194	291	0.70 (0.55-0.84)	0.38 (0.26-0.48)	0.50 (0.35-0.64)	0.46 (0.37-0.56)	0.45 (0.31-0.57)	0.99 (0.70-1.25)	
2010-2015	184	172	0.66 (0.40-0.91)	0.24 (0.00-0.47)	0.40 (0.15-0.65)	0.40 (0.24-0.56)	0.27 (0.00-0.52)	0.73 (0.25-1.18)	
2010-2020 ‡	-	-	<i>0.63</i> (0.36-0.89)	<i>0.23</i> (-0.05-0.50)	<i>0.38</i> (0.11-0.65)	<i>0.37</i> (0.21-0.53)	<i>0.25</i> (-0.05-0.54)	<i>0.68</i> (0.17-1.16)	
2020-2030 ‡	-	-	<i>0.59</i> (0.24-0.93)	<i>0.12</i> (-0.29-0.51)	<i>0.30</i> (-0.08-0.67)	<i>0.31</i> (0.13-0.49)	<i>0.12</i> (-0.29-0.52)	<i>0.47</i> (-0.15-1.07)	
2030-2040 ‡	-	-	<i>0.55</i> (0.08-0.99)	<i>0.00</i> (-0.54-0.49)	<i>0.21</i> (-0.29-0.67)	<i>0.26</i> (0.04-0.47)	<i>0.00</i> (-0.50-0.46)	<i>0.29</i> (-0.46-0.97)	

712 * Total Continental C sink is the per unit area aboveground C sink multiplied by intact forest area for
713 1990-2010 (from ref.¹, see Extended Data Table 2) and continent specific extrapolations to 2040. Total
714 Continental C sink includes continent-specific estimates of trees <100 mm DBH, lianas and roots (see
715 Methods).

716 † Pan-tropical aboveground live biomass C sink is the area-weighted mean of African, Amazonian and
717 Southeast Asian sink values. Southeast Asian values were from published per unit area carbon sink
718 data¹⁵ (n=49 plots) for 1990-2015, with 1980-1990 assumed to be the same as 1990-2000 due very low
719 sample sizes. Pan-tropical total C sink is the sum of African, Amazonian and Southeast Asian total
720 continental carbon sink values. The continental sink in Southeast Asia is a modest and declining
721 contribution to the pan-tropical sink, due to the very small area of intact forest remaining, at 0.11, 0.08,
722 0.07 and 0.06 Pg C yr⁻¹ in the 1980s, 1990s, 2000s and 2010s, hence uncertainty in the Southeast Asian
723 sink cannot reverse the pan-tropical declining sink trend.

724 ‡ Per unit area total C sink for 2010-2020, 2020-2030 and 2030-2040 was predicted using parameters
725 from Table 2, except for the 2010-2020 sink in Africa which is the mean of the measured sink from
726 2010-2015 and the modelled sink from 2015-2020. For the Asian sink we assumed the parameters as
727 for Africa, as Asian forest median CRT is 61 years, close to African median, 63 years.

728

729 **Table 2. Minimum adequate models to predict carbon gains and losses in African and**
 730 **Amazonian tropical forests. These are the best ranked gains and loss models.** Where continental
 731 values differ, those for Africa are reported first, followed by Amazonian values.

Carbon gains, Mg C ha ⁻¹ yr ⁻¹						
Predictor variable	Parameter value	Standard Error	t-value	p-value	2000-2015 change in gains (%) *	
(Intercept)	5.255 5.395	0.603 0.614	8.7 8.8	<0.001	-	
CO ₂ -change (ppm yr ⁻¹) †	0.238	0.096	2.5	0.013	3.69% 3.71%	
MAT (°C)	-0.083	0.025	-3.3	0.001	-0.67% -1.07%	
MAT-change (°C yr ⁻¹) ‡	-1.243	0.233	-5.3	<0.001	0.58% 0.00% §	
MCWD (mm x1000)	-0.405 -1.391	0.381 0.24	-1.1 -5.8	0.289 <0.001	-0.52% -2.73%	
WD (g cm ⁻³)	-1.295	0.530	-2.4	0.015	0.05% 0.00%	
Carbon losses, Mg C ha ⁻¹ yr ⁻¹						
Predictor variable	Parameter value	Standard Error	t-value	p-value	2000-2015 change in losses (%) *	
(Intercept)	1.216	0.086	14.1	<0.001	-	
CO ₂ -change (ppm yr ⁻¹) †	0.130	0.059	2.2	0.026	11.38% 14.81%	
MAT-change (°C yr ⁻¹) ‡	0.766	0.162	4.7	<0.001	-1.56% 0.00%	
MCWD (mm x10000) ‡	-0.232	0.107	-2.2	0.030	-1.21% -2.42%	
CRT (yr)	-0.003	0.001	-6.1	<0.001	-0.57% 1.39%	

732 * The 2000-2015 change in gains/losses for each predictor variable was estimated allowing only the
 733 focal predictor to vary; this change was then expressed as a percentage of the annual gains/losses in
 734 the year 2000 allowing all predictors to vary.

735 † Change over the past 56 years.

736 ‡ Change over the past 5 years.

737 § A positive value for Africa indicates that MAT increased more slowly over 2000-2015 compared to
 738 the mean increase over 1983-2015, therefore contributing to an increase in gains; a zero value for
 739 Amazonia indicates that the rate of MAT increase was the same over 2000-2015 as the mean increase
 740 over 1983-2015.

741 || Carbon loss values were normalized via power-law transformation, $\lambda = 0.361$.

742

743 **Online Methods**

744

745 **Plot Selection**

746 Closed canopy (i.e. not woody savanna) old-growth mixed-age forest inventory plots were selected
747 using commonly used criteria^{6,13,27}: free of fire and industrial logging; all trees with diameter at
748 reference height ≥ 100 mm measured at least twice; ≥ 0.2 ha area; < 1500 m.a.s.l. altitude; MAT
749 $\geq 20.0^\circ\text{C}^{51}$; annual precipitation ≥ 1000 mm⁵¹; located ≥ 50 m from anthropogenic forest edges. Of the
750 244 plots included in the study, 217 contribute to the African Tropical Rainforest Observatory Network
751 (AfriTRON; www.afritron.org), with data curated at www.ForestPlots.net^{52,53}. These include plots
752 from Sierra Leone, Liberia, Ghana, Nigeria, Cameroon, Gabon, Republic of Congo, Democratic
753 Republic of Congo (DRC), Uganda and Tanzania^{52,53} (Extended Data Figure 1). Fifteen plots are part
754 of the TEAM network, from Cameroon, Republic of Congo, Tanzania, and Uganda⁵⁴⁻⁵⁷. Nine plots
755 contribute to the ForestGEO network, from Cameroon and DRC⁵⁸ (9 plots from DRC, codes SNG,
756 contribute to both AfriTRON and ForestGEO networks, included above in the AfriTRON total).
757 Finally, three plots from Central African Republic are part of the CIRAD network^{59,60}. The large
758 majority of plots are sited in terra firme forests and have mixed species composition, although four are
759 in seasonally flooded forest and 14 plots are in *Gilbertiodendron dewevrei* monodominant forest, a
760 locally common forest type in Africa (Supplementary Table 1). The 244 plots have a mean size of 1.1
761 ha (median, 1 ha), with a total plot area of 277.9 ha. The dataset comprises 391,968 diameter
762 measurements on 135,625 stems, of which 89.9% were identified to species, 97.5% to genus and 97.8%
763 to family. Mean total monitoring period is 11.8 years, mean census length 5.7 years, with a total of
764 3,214 ha years of monitoring. The 321 Amazon plots are published and were selected using the same
765 criteria⁶, except in the African selection criteria we specified a minimum anthropogenic edge distance
766 and added a minimum temperature threshold.

767

768 **Plot Inventory and Tree Biomass Carbon Estimation**

769 Tree-level aboveground biomass carbon is estimated using an allometric equation with parameters for
770 tree diameter, tree height and wood mass density⁶¹. The calculation of each is discussed in turn. All
771 calculations were performed using the R statistical platform, version 3.2.1 (ref.⁶²) using the BiomasaFP
772 R package, version 0.2.1 (ref.⁶³).

773

774 *Tree Diameter:* In all plots, all woody stems with ≥ 100 mm diameter at 1.3 m from the base of the
775 stem ('diameter at breast height', DBH), or 0.5 m above deformities or buttresses, were measured,
776 mapped and identified using standard forest inventory methods^{64,65}. The height of the point of
777 measurement (POM) was marked on the trees and recorded, so that the same POM is used at the
778 subsequent forest census. For stems developing deformities or buttresses over time that could
779 potentially disturb the initial POM, the POM was raised approximately 500 mm above the deformity.
780 Estimates of the diameter growth of trees with changed POM used the ratio of new and old POMs, to
781 create a single trajectory of growth from the series of diameters at two POM heights^{6,13,65}. We used
782 standardised protocols to assess typographical errors and potentially erroneous diameter values (e.g.
783 trees shrinking by >5 mm), missing values, failures to find the original POM, and other issues. Where
784 necessary we estimated the likely value via interpolation or extrapolation from other measurements of
785 that tree, or when this was not possible we used the median growth rate of trees in the same plot, census
786 and size-class, defined as DBH = 100-199 mm, or 200-399 mm, or >400 mm⁶⁵. We interpolated
787 measurements for 1.3% of diameters, extrapolated 0.9%, and used median growth rates for 1.5%.

788

789 *Tree height:* Height of individuals from ground to the top leaf, hereafter H_t , was measured in 204 plots,
790 using a laser hypsometer (Nikon forestry Pro) from directly below the crown (most plots), a laser or
791 ultrasonic distance device with an electronic tilt sensor, a manual clinometer, or by direct
792 measurement, i.e. tree climbing. Only trees where the top was visible were selected⁶⁶. In most plots,

793 tree selection was similar: the 10 largest trees were measured, together with 10 randomly selected trees
794 per diameter from five classes: 100-199 mm, 200-299 mm, 300-399 mm, 400-499 mm, and 500+ mm
795 trees, following standard protocols⁶⁶. We measured actual height of 24,270 individual trees from 204
796 plots. We used these data and the local.heights function in R package BiomasaFP⁶³ to fit 3-parameter
797 Weibull relationships: $H_t = a \times (1 - e^{-(b \times (DBH/10)^c)})$ (equation 1). We chose the Weibull model as it is
798 known to be robust when a large number of measurements are available^{66,67}. We parameterised
799 separate H_t -DBH relationship for four different combinations of edaphic forest type and
800 biogeographical region: (i) terra firme forest in West Africa, (ii) terra firme forest in Lower Guinea
801 and Western Congo Basin, (iii) terra firme forest in Eastern Congo Basin and East Africa, (iv)
802 seasonally flooded forest from Lower Guinea and Western Congo Basin (there were no seasonally
803 flooded forest plots in the other biogeographical regions). The parameters are: (i) terra firme forest in
804 West Africa, $a=56.0$; $b=0.0401$; $c=0.744$; (ii) terra firme forest in Lower Guinea and Western Congo
805 Basin, $a=47.6$; $b=0.0536$; $c=0.755$; (iii) terra firme forest in Eastern Congo Basin and East Africa,
806 $a=50.8$; $b=0.0499$; $c=0.706$; and finally (iv) seasonally flooded forest from Lower Guinea and Western
807 Congo Basin, $a=38.2$; $b=0.0605$; $c=0.760$. For each of these combinations of forest type and bioregion,
808 the local.heights function combines all height measurements from all plots belonging to that forest
809 type/bioregion and fits the Weibull model parameters using non-linear least squares (nls function in R
810 with default settings), with starting values of $a = 25$, $b = 0.05$ and $c = 0.7$ chosen as they led to regular
811 model convergence. We fitted these models either treating each observation equally or with case
812 weights proportional to each trees' basal area. These weights give more importance to large trees
813 during model fitting. We selected the best fitting of these models, determining this as the model that
814 minimised prediction error of stand biomass when calculated with estimated heights or observed
815 heights. The parameters were used to estimate H_t from DBH for all tree DBH measurements for input
816 into the allometric equation. Mean measured individual total tree height is 20.5 m; the height range is
817 1.5 to 72.5 m. The root mean squared error (RMSE) between the full dataset of measured heights and

818 the predicted heights, is 5.7 m, which is 8.0% of the total range. Furthermore, RMSE is 5.3 m in terra
819 firme forest in West Africa (7.5% of the range; n=9771 trees); RMSE is 6.4 m in terra firme forest in
820 Lower Guinea and Western Congo Basin (8.7% of the range; n=10,838 trees); RMSE is 4.8 m in terra
821 firme forest in Eastern Congo Basin and East Africa (8.8% of the range; n=3269 trees); and RMSE is
822 4.1 m in seasonally flooded forest from Lower Guinea and Western Congo Basin (12.5% of the range;
823 n=392 trees).

824

825 *Wood Density:* Dry wood density (ρ) measurements were compiled for 730 African species from
826 published sources and stored in www.ForestPlots.net; most were sourced from the Global Wood
827 Density Database on the Dryad digital repository (www.datadryad.org)^{68,69}. Each individual in the tree
828 inventory database was matched to a species-specific mean wood density value. Species in both the
829 tree inventory and wood density databases were standardized for orthography and synonymy using the
830 African Plants Database (www.ville-ge.ch/cjb/bd/africa/) to maximize matches¹³. For incompletely
831 identified individuals or for individuals belonging to species not in the ρ database, we used the mean
832 ρ value for the next higher known taxonomic category (genus or family, as appropriate). For
833 unidentified individuals, we used the mean wood density value of all individual trees in the plot^{13,52}.

834

835 *Allometric equation:* For each tree we used a published allometric equation⁶¹ to estimate aboveground
836 biomass. We then converted this to carbon, assuming that aboveground carbon (AGC) is 45.6% of
837 aboveground biomass⁷⁰. Thus: $AGC = 0.456 \times (0.0673 \times (\rho \times (DBH/10)^2 \times H_i)^{0.976}) / 1000$ (equation 2), with
838 DBH in mm, dry wood density, ρ , in $g\ cm^{-3}$, and total tree height, H_i , in m (ref.⁶¹).

839

840 *Aboveground Carbon* (AGC, in $Mg\ C\ ha^{-1}$) in living biomass for each plot at each census date was
841 estimated as the sum of the AGC of each living stem, divided by plot area (in hectares).

842

843 **Carbon Gain and Carbon Loss estimation**

844 *Net Carbon Sink* (in Mg C ha⁻¹ yr⁻¹) is estimated as carbon gains minus carbon losses. Calculation
845 details are explained below.

846

847 *Carbon Gains* (in Mg C ha⁻¹ yr⁻¹) are the sum of the aboveground live biomass carbon additions from
848 the growth of surviving stems and the addition of newly recruited stems, divided by the census length
849 (in years) and plot area (in hectares). For each stem that survived a census interval, carbon additions
850 from its growth (Mg C ha⁻¹ yr⁻¹) were calculated as the difference between its AGC at the end census
851 of the interval and its AGC at the beginning census of the interval. For each stem that recruited during
852 the census interval (i.e. reaching DBH \geq 100 mm), carbon additions were calculated in the same way,
853 assuming DBH=0 mm at the start of the interval⁶⁵. *Carbon Losses* (in Mg C ha⁻¹ yr⁻¹) are estimated as
854 the sum of aboveground biomass carbon from all stems that died during a census interval, divided by
855 the census length (in years) and plot area (in hectares). Both carbon gains and carbon losses are
856 calculated using standard methods⁶, including a census interval bias correction, using the
857 SummaryAGWP function of R-package BiomasaFP^{63,64,68}.

858

859 As carbon gains are affected by a census interval bias, with the underestimate increasing with census
860 length, we corrected this bias by accounting for (i) the carbon additions from trees that grew before
861 they died within an interval (unobserved growth) and (ii) the carbon additions from trees that recruited
862 and then died within the same interval (unobserved recruitment)^{65,71}.

863

864 Component (i), the unobserved growth of a stem that died during a census interval, is estimated as the
865 difference between AGC at death and AGC at the start of the census. These are calculated using
866 equation 2, from respectively DBH_{death} and DBH_{start}. The latter is part of the data, the first can be
867 estimated as: $DBH_{\text{death}} = DBH_{\text{start}} \times G \times Y_{\text{mean}}$, where G is the plot-level median diameter growth rate

868 (mm yr⁻¹) of the size class the tree was in at the start of the census interval (size classes are defined as
869 $D < 200$ mm, $400 \text{ mm} > D \geq 200$ mm and $D \geq 400$ mm) and Y_{mean} is the mean number of years trees
870 survived in the census interval before dying. Y_{mean} is calculated from the number of trees that are
871 expected to have died in each year of the census interval, which is derived from the plot-level per-
872 capita mortality rate (m_a ; % dead trees yr⁻¹) calculated following equation 5 in ref.⁷¹.

873

874 Component (ii), growth of recruits that were not observed because they died during the census interval,
875 is estimated by calculating the number of unobserved recruits and diameter at death for each
876 unobserved recruit. The number of unobserved recruits (stems ha⁻¹ yr⁻¹) is estimated as: $N_{u,r} = R_a -$
877 $P_{\text{surv}} \times R_a$, where R_a (recruited stems ha⁻¹ yr⁻¹) is the per area annual recruitment calculated following
878 equation 11 in ref.⁷¹ and P_{surv} is the probability of each recruit surviving until the next census: $P_{\text{surv}} =$
879 $(1 - m_a)^T$, where T is the number of years remaining in the census interval. Summing $N_{u,r}$ for each year
880 in a census interval gives the total number of unobserved recruits in that census interval. We then
881 estimate diameter at death for each unobserved recruit, which is given in mm by $\text{DBH}_{\text{death},u,r} = 100 +$
882 $(G_s \times Y_{\text{mean-rec}})$, where G_s is the plot-level median diameter growth rate (mm yr⁻¹) of the smallest size
883 class (i.e. $D < 200$ mm) and $Y_{\text{mean-rec}}$ is the mean life-span of unobserved recruits calculated as the
884 mean life-span of recruits in a given year, weighted by $N_{u,r}$. The mean life-span of recruits in a given
885 year is calculated from the number of recruits that died in that year, which is derived from the plot-
886 level per-capita mortality rate (m_a ; % dead trees yr⁻¹). Growth of each unobserved recruit (mm yr⁻¹) is
887 then calculated as $\text{DBH}_{\text{death},u,r}$ divided by $Y_{\text{mean-rec}}$.

888

889 The census interval bias correction (components i and ii together) typically add <3% to plot-level
890 carbon gains. Carbon Losses are affected by the same census interval bias, hence we corrected this
891 bias by accounting for (i) the additional carbon losses from the trees that were recruited and then died
892 within the same interval, and (ii) the additional carbon losses resulting from the growth of the trees

893 that died in the interval^{6,15,63}. These two components are calculated in the same way as for Carbon
894 gains and typically add <3% to plot-level carbon losses.

895

896 Carbon gains include both gains from the growth of surviving stems and new recruits. Separating
897 carbon gains from tree growth of surviving stems and newly recruited stems, shows that carbon gains
898 from recruitment are small overall, and are significantly lower in Africa than in the Amazon, likely
899 due to the lower stem turnover rates and longer carbon residence time (Africa: 0.17 Mg C ha⁻¹ yr⁻¹; CI:
900 0.16-0.18 versus Amazon: 0.27 Mg C ha⁻¹ yr⁻¹; CI: 0.25-0.28, p<0.001; two-way Wilcoxon test), but
901 this is compensated by carbon gains from survivors being significantly larger in Africa (2.33 Mg C ha⁻¹
902 yr⁻¹; CI: 2.27-2.39) than in the Amazon (2.13 Mg C ha⁻¹ yr⁻¹; CI: 2.09-2.17, p=0.014). Therefore,
903 gains overall (sum of gains from surviving stems and newly recruited stems) are indistinguishable
904 between the continents (Africa: 2.57 Mg C ha⁻¹ yr⁻¹; CI: 2.51-2.67 vs Amazon: 2.46 Mg C ha⁻¹ yr⁻¹; CI:
905 2.41-2.50, p=0.460; two-way Wilcoxon test).

906

907 **Long-term Gain, Loss and Net Carbon Sink Trend Estimation, 1983-2014**

908 The estimated mean and uncertainty in carbon gains, carbon losses and the net carbon sink of the
909 African plots from 1983-2014 (Figure 1, Extended Data Figure 7 and Extended Data Figure 8) were
910 calculated following ref.⁶ to allow direct comparison with published Amazonian results. First, each
911 census interval value was interpolated for each 0.1-yr period within the census interval. Then, for each
912 0.1-yr period between 1983 and 2014, we calculated a weighted mean of all plots monitored at that
913 time, using the square root of plot area as a weighting factor⁶. Confidence intervals for each 0.1-yr
914 period were bootstrapped.

915

916 Trends in carbon gains, losses and the net carbon sink over time were assessed using linear mixed
917 effects models (lmer function in R, lme4 package⁷²), providing the linear slopes reported in Figure 1.

918 These models regress the mid-point of each census interval against the value of the response variable
919 for that census interval. Plot identity was included as a random effect, i.e. assuming that the intercept
920 can vary randomly among plots. We did not include slope as a random effect, consistent with
921 previously published Amazon analyses⁶, because models did not converge due to some plots having
922 too few census intervals. Observations were weighted by plot size and census interval length.
923 Weightings were derived empirically, by assuming *a priori* that there is no significant relation between
924 the net carbon sink and census interval length or plot size, following ref.¹³. The following weighting
925 removes all pattern in the residuals: $\text{Weight} = \sqrt[3]{\text{length}_{\text{int}}} + \sqrt[4]{\text{plotsize} - 1}$ (equation 3), where $\text{length}_{\text{int}}$ is
926 the length of the census interval, in years. Significance was assessed by regressing the residuals of the
927 net carbon sink model against the weights ($p=0.702$).

928

929 Differences in long-term slopes between the two continents for carbon gains, carbon losses and net
930 carbon sink, reported in the main text, were also assessed using linear mixed effects models, as
931 described above, but performed on the combined African and Amazonian datasets and limited to their
932 common time window, 1983 to 2011.5. For these three tests on the pooled data we included an
933 additional interaction term between census interval date and continent, where a significant interaction
934 would indicate that the slopes differ between continents. The statistical significance of continental
935 differences in slope were assessed using the F-statistic (Anova function in R, car package⁷³).
936 Shortening the common time window to the 20 years when the continents are best-sampled, 1991.5 to
937 2011.5, gave very similar results, including a divergent continental sink ($p=0.04$).

938

939 **Continental and Pan-Tropical Carbon Sink Estimates**

940 The *per unit area total net carbon sink* (in $\text{Mg C ha}^{-1} \text{ yr}^{-1}$) for each time period in Table 1 (each decade
941 between 1980 and 2010; and 2010-2015) is the sum of three components. The first component is the
942 per unit area aboveground carbon sink from living trees and lianas with $\text{DBH} \geq 100$ mm. For Africa we

943 use the per unit area net carbon sink values presented in this paper. For Amazonia, we use data in ref.⁶.
944 For Southeast Asia, we use inventory data collected using similar standardised methods from 49 plots
945 in ref.¹⁵. For each time window, we use all plots for which census dates overlap the period, weighted
946 by the square root of plot area, as for the solid lines in Figure 1. The second component is the per unit
947 area aboveground carbon sink from living trees and lianas with DBH<100 mm. This is calculated as
948 5.19%, 9.40% and 5.46% of the first component (i.e. aboveground carbon of large living trees) in
949 Africa, Amazonia and Southeast Asia respectively^{13,74}. The third component is the per unit area
950 belowground carbon sink in live biomass, i.e. roots. This is calculated as 25%, 37% and 17% of the
951 aboveground carbon of living trees with DBH≥100 mm in Africa¹³, Amazonia⁶ and Southeast Asia⁷⁵
952 respectively.

953

954 For each time period in Table 1 we calculated the *continental-scale total carbon sink* (Pg C yr⁻¹) by
955 multiplying the per unit area total net carbon sink described above by the area of intact forest on each
956 continent at that time interval (in ha) reported in Extended Data Table 2. Decades are calculated from
957 1990.01 to 1999.99. For comparability with previous continental-sink results, we used continental
958 values of intact forest area for 1990, 2000 and 2010 as published in ref.¹, *i.e.* total forest area minus
959 forest regrowth. We used the 1990-2010 data to fit an exponential model for each continent and used
960 this model to estimate intact forest area for 1980 and 2015.

961

962 Finally, in the main text we calculated the proportion of anthropogenic CO₂ emissions removed by Earth's intact
963 tropical forests, as the total pan-tropical carbon sink from Table 1 divided by the total anthropogenic CO₂
964 emissions. Total anthropogenic CO₂ emissions are calculated as the sum of emissions from fossil fuel and land-
965 use change and are estimated at 7.6 Pg C yr⁻¹ in the 1990s, 9.0 Pg C yr⁻¹ in the 2000s, and 11.1 Pg C yr⁻¹ in the
966 2010s (ref.²¹, assuming 1.7% growth in fossil fuel emissions in 2018 and 2019, and mean 2010-2017 land-use
967 change emissions for 2018 and 2019).

968

969 **Carbon Sink from an Atmospheric Perspective**

970 To estimate the evolution of the carbon sink from an atmospheric perspective, we assumed that the
971 contribution to the atmosphere from carbon gains are experienced immediately, while the contribution
972 to the atmosphere from carbon losses must take into account the delay in decomposition of dead trees.
973 We did this by calculating total forest carbon loss ($\text{Mg C ha}^{-1} \text{ yr}^{-1}$) for each year between 1950-2015,
974 using the mean 1983-2015 records from Figure 1 and assuming constant losses prior to 1983 (1.9 and
975 $1.5 \text{ Mg C ha}^{-1} \text{ yr}^{-1}$ for Africa and Amazonia respectively). Then, for each focal year between 1950-
976 2015, we calculated how much carbon was released to the atmosphere in the subsequent years as: $y_t =$
977 $x_0 \times e^{-0.17 \times (t-1)} - x_0 \times e^{-0.17 \times t}$, where x_0 is the total forest carbon loss of the focal year; y_t is the carbon
978 released to the atmosphere at t years from the focal year; and -0.17 yr^{-1} is a constant decomposition
979 rate calculated for tropical forests in the Amazon⁴⁵. For example, carbon loss was $1.95 \text{ Mg C ha}^{-1}$ in
980 1990 in African forests (Figure 1), from which $0.31 \text{ Mg C ha}^{-1}$ was released to the atmosphere in 1991;
981 $0.26 \text{ Mg C ha}^{-1}$ in 1992; $0.22 \text{ Mg C ha}^{-1}$ in 1993; $0.07 \text{ Mg C ha}^{-1}$ in 2000 and $0.01 \text{ Mg C ha}^{-1}$ in 2010.
982 Hence, of the full $1.95 \text{ Mg C ha}^{-1}$ dead tree biomass from 1990, $\sim 50\%$ was released to the atmosphere
983 after 4 yrs, $\sim 85\%$ after 10 yrs, and $\sim 97\%$ after 20 years. Finally, for each year between 1983 and 2015,
984 the total contribution to the atmosphere from carbon losses was calculated as the sum of all carbon
985 contributions released at that year, from all total yearly forest carbon loss pools of the previous years.
986 We then calculated decadal-scale mean contributions to the atmosphere from carbon losses, reported
987 in the main text.

988

989 **Predictor Variable Estimates, 1983-2014**

990 For each census interval of each plot, we examined potential predictor variables that may explain the
991 long-term trends in carbon gains and carbon losses, reported in Extended Data Table 1 and main text
992 Table 2. First, the environmental conditions during the census interval; second the rate of change of
993 these parameters; and third forest attributes that may affect how different forests respond to the same

994 environmental change. The predictor variable estimates for each census need to avoid bias due to
995 seasonal variation, for example the intra-annual variability in atmospheric CO₂ concentration. We
996 therefore applied the following procedure to avoid seasonal variability impacts on long-term trends:
997 (i) the length of each focal census interval was rounded to the nearest complete year (e.g. a 1.1 year
998 interval became a 1 year interval); (ii) we computed dates that minimised the difference between actual
999 fieldwork dates and complete-year census dates, while ensuring that subsequent census intervals of a
1000 plot do not overlap. The resulting sequence of non-overlapping census intervals was used to calculate
1001 interval-specific means for each environmental predictor variable to remove seasonal effects. The
1002 mean difference between the actual fieldwork dates and the complete-year census dates is 0.01 decimal
1003 years.

1004

1005 The first group of potential predictor variables, estimated for each census interval of each plot, are
1006 theory-driven choices: atmospheric CO₂ concentration (CO₂), mean annual temperature (MAT), and
1007 drought intensity, which we quantified as maximum climatological water deficit (MCWD)^{14,20,76,77}.

1008

1009 *Atmospheric CO₂ concentration* (CO₂, in ppm) is estimated as the mean of the monthly mean values
1010 from the Mauna Loa record⁷⁸ over the census interval. While atmospheric CO₂ concentration is highly
1011 correlated with time (R²=0.98), carbon gains are slightly better correlated with CO₂ (R_{adj}²=0.0027)
1012 than with time (R_{adj}²=0.0025).

1013

1014 *Mean Annual Temperature* (MAT, in °C) was derived from the temporally resolved (1901-2015)
1015 dataset of monthly mean temperature from the Climatic Research Unit (CRU TS version 4.03; ~3025
1016 km² resolution; released 15 May 2019; <https://crudata.uea.ac.uk/cru/data/hrg/>)⁷⁹. We downscaled the
1017 data to ~1 km² resolution using the WorldClim dataset^{51,80}, by subtracting the difference in mean

1018 monthly temperature, and applying this monthly correction to all months⁸¹. We then calculated MAT
1019 for each census interval of each plot using the downscaled monthly CRU record.

1020

1021 *Maximum Climatological Water Deficit* (MCWD, in mm) was derived from the ~3025 km² resolution
1022 Global Precipitation Climatology Centre dataset (GPCC version 6.0) that includes many more rain
1023 gauges than CRU in tropical Africa^{82,83}. As GPCC ends in 2013 we combined it with satellite-based
1024 Tropical Rainfall Measurement Mission data (TRMM 3B43 V7 product, ~757 km² resolution)⁸⁴. The
1025 fit for the overlapping time period (1998-2013) was used to correct the systematic difference between
1026 GPCC and TRMM: $GPCC' = a + b * GPCC$, with GPCC' the adjusted GPCC record and a and b different
1027 parameters for each month of the year and for each continent. Precipitation was then downscaled to ~1
1028 km² resolution using the WorldClim dataset^{51,80}, by dividing by the ratio in mean monthly rainfall, and
1029 applying this monthly correction to all months⁸¹. For each census interval we extracted monthly
1030 precipitation values and estimated evapotranspiration (ET) to calculate monthly Climatological Water
1031 Deficit (CWD), a commonly used metric of dry season intensity for tropical forests^{14,76,77}. Monthly
1032 CWD values were calculated for each subsequent series of 12 months (complete years)⁷⁷. Monthly
1033 CWD estimation begins with the wettest month of the first year in the interval, and is calculated as 100
1034 mm per month evapotranspiration (ET) minus monthly precipitation (P). Then, CWD values for the
1035 subsequent 11 months were calculated recursively as: $CWD_i = ET - P_i + CWD_{i-1}$, where negative CWD_i
1036 values were set to zero⁷⁷ (no drought conditions). This procedure was repeated for each subsequent
1037 complete 12 months. We then calculated the annual MCWD as the largest monthly CWD value for
1038 every complete year within the census interval, with the MCWD of a census interval being the mean
1039 of the annual MCWD values within the census interval. Larger MCWD indicates more severe water
1040 deficits.

1041

1042 We assume ET is 100 mm month⁻¹ on both continents, based on measurements from Amazonia^{76,77},
1043 more limited measurements from West Africa summarized in ref.⁸⁵, predictive skill⁸⁶, and use in past
1044 studies on both continents^{14,87}. MCWD therefore represents a precipitation-driven dry season deficit,
1045 as ET remains constant. An alternative assessment, using a data-driven ET product^{88,89}, gave a mean
1046 ET of 95 and 98 mm month⁻¹ for the African and Amazonian plot networks respectively. Using these
1047 values did not affect the results.

1048

1049 To calculate the environmental change of potential predictor variables, CO₂-change (in ppm yr⁻¹),
1050 MAT-change (in °C yr⁻¹) and MCWD-change (in mm yr⁻¹), we selected an optimum period over which
1051 to calculate the change, derived empirically by assessing the correlation of carbon gains (all plots, all
1052 censuses) with the change in each environmental variable, using linear mixed effects models (lmer
1053 function in R, lme4 package⁷²). The annualised change in the environmental variable was calculated
1054 as the change between the focal interval and a prior interval (termed the baseline period) with a
1055 lengthening time window ranging from 1 year through to 80 years prior to the focal interval (i.e. 80
1056 linear mixed effects models per variable). We calculated AIC for each model and selected the interval
1057 length with the lowest AIC. Thus, MAT-change (in °C yr⁻¹) = (MAT_i-MAT_b)/(date_i-date_b), where
1058 MAT_i is the MAT over the focal census interval calculated using the procedure described above, MAT_b
1059 is the MAT over a baseline period prior to the focal interval, date_i is the mid-date of the focal census
1060 interval and date_b is the mid-date of the baseline period. The lmer results show that the baseline period
1061 for MAT-change is 5 years and for CO₂-change it is 56 years, while MCWD showed no clear trend,
1062 so MCWD-change was not included in the models (see Extended Data Figure 3). All three results
1063 conform to *a priori* theoretical expectations. For CO₂ a maximum response to an integrated 56 years
1064 of change is expected because forest stands will respond most strongly to CO₂ when most individuals
1065 have grown under the new rapidly changing condition, which should be at its maximum at a time
1066 approximately equivalent to the carbon residence time of a forest stand^{30,90} (mean of 62 years in this

1067 dataset). For MAT, 5 years is consistent with experiments showing temperature acclimation of leaf-
1068 and plant-level photosynthetic and respiration processes over half-decadal timescales^{31,91}. MCWD has
1069 no overall trend suggesting that once a drought ends, its impact on tree growth fades rapidly, as seen
1070 in other studies^{14,92}. Also in the moist tropics wet-season rainfall is expected to re-charge soil water,
1071 hence lagged impacts of droughts are not expected.

1072

1073 We calculated estimates of two forest attributes that may alter responses to environmental change as
1074 potential predictor variables: Wood Density (WD) and Carbon Residence Time (CRT). In intact old-
1075 growth forests, mean WD (in g cm^{-3}) is inversely related to resource availability^{28,93,94}, as is seen in
1076 our dataset (carbon gains and plot-level mean WD are negatively correlated, Extended Data Figure 4).
1077 WD is calculated for each census interval in the dataset, as the mean WD of all trees alive at the end
1078 of the census interval, to be consistent with the previous Amazon analysis⁶. Carbon residence time
1079 (CRT, in yrs) is a measure of the time that fixed carbon stays in the system. CRT is a potential correlate
1080 of the impact of past carbon gains on later carbon losses³⁰. To avoid circularity in the models, the
1081 equation used to calculate CRT differed depending on the response variable. If the response variable
1082 is carbon loss, the CRT equation is based on gains: $\text{CRT} = \text{AGC} / \text{gains}$, with AGC for each interval
1083 based on AGC at the end of the interval, and the gains for each interval calculated as the mean of the
1084 gains in the interval and the previous intervals (i.e. long-term gains). If the response variable is carbon
1085 gains, the CRT equation is based on losses: $\text{CRT} = \text{AGC} / \text{losses}$. The equation employed for use in the
1086 carbon loss model (based on gains) is the standard formula used to calculate CRT and is retained in
1087 the minimum adequate model (see below and Table 2). The non-standard CRT equation (based on
1088 losses) used in the carbon gain model is not retained in the minimum adequate model (see below).

1089

1090 **Statistical modelling of the Carbon Gain, Loss and Sink Trends**

1091 We first constructed two models including those environmental drivers exhibiting long-term change
1092 that impact theory-driven models of photosynthesis and respiration as predictor variables: CO₂, MAT,
1093 and MCWD. One model had carbon gains as the response variable, the other had carbon losses as the
1094 response variable (both in Mg C ha⁻¹ yr⁻¹). Models were fitted using the lme function in R, with
1095 maximum likelihood (NLME package⁹⁵). All census intervals within all plots were used, weighted by
1096 plot size and census length (using equation 3 above). Plot identity was included as a random effect,
1097 i.e. assuming that the intercept can vary randomly among plots. All predictor variables in the models
1098 were scaled without centering (scale function in R, RASTER package⁶²). Carbon gain values were
1099 normally distributed but carbon loss values required a power-law transformation ($\lambda= 0.361$) to meet
1100 normality criteria. Multi-parameter models are: carbon gains = intcp + a×CO₂ + b×MAT + c×MCWD
1101 (model 1); carbon losses = intcp + a×CO₂ + b×MAT + c×MCWD (model 2); where intcp is the
1102 estimated model intercept, and a, b, and c are model parameters giving the slope of relationships with
1103 environmental predictor variables. For multi-parameter model outputs see Extended Data Table 1, for
1104 single-parameter relationships, Figure 2.

1105

1106 The second pair of models include the same environmental predictors (CO₂, MAT, MCWD), plus their
1107 rate of change (CO₂-change, MAT-change, but not MCWD-change as explained above), and forest
1108 attributes that may alter how forests respond (WD, CRT), as described above. We also evaluated the
1109 possible inclusion of a differential continent effect of each variable in the full model. We first
1110 constructed models with only a single predictor variable, and allowed different slopes in each
1111 continent. Next, if removal of the continent-specific slope (using stepAIC function in R, MASS
1112 package⁹⁶) decreased model Akaike Information Criterion (AIC) then the continent-specific slope was
1113 not included in the full model for that variable. Only MCWD showed a significant differential
1114 continent-specific slope. This implies that forests on both continents have common responses to CO₂,

1115 CO₂-change, MAT, MAT-change, WD and CRT, but respond differently to differences in MCWD.
1116 This is likely because wet-adapted species are much rarer in Africa than in Amazonia as a result of
1117 large differences in past climate variation³⁴. Lastly, we allowed different intercepts for the two
1118 continents to potentially account for differing biogeographical or other continent-specific factors. For
1119 the carbon loss model, we applied the same continent-specific effects for slope as for the carbon gain
1120 model. Carbon loss values were transformed using a power-law transformation ($\lambda = 0.361$) to meet
1121 normality criteria.

1122

1123 For both carbon gains and losses we parameterized a global model including the significant continent-
1124 specific effect of MCWD, selecting the most parsimonious simplified model using all-subsets
1125 regression^{97,98}. To do so, we first generated a set of models with all possible combinations (subsets) of
1126 fixed effect terms in the global model using the dredge function of the MuMIn package in R⁹⁹. We
1127 then chose the best-ranked simplified model based on the AICc criterion, hereafter called “minimum
1128 adequate carbon gain/loss model”, reported in Table 2. The minimum adequate models are: carbon
1129 gains = $\text{intcp} \times \text{continent} + a \times \text{CO}_2\text{-change} + b \times \text{MAT} + c \times \text{MAT-change} + d \times \text{MCWD} \times \text{continent} +$
1130 $e \times \text{WD}$ (model 3); carbon losses = $\text{intcp} + a \times \text{CO}_2\text{-change} + b \times \text{MAT-change} + c \times \text{MCWD} + d \times \text{CRT}$
1131 (model 4). WD was retained in the carbon gain model, likely because growth is primarily impacted by
1132 resource availability, while CRT was retained in the carbon loss model, likely because losses are
1133 primarily impacted by how long fixed carbon is retained in the system.

1134

1135 Table 2 presents model coefficients of the best-ranked gain model and best-ranked loss model selected
1136 using all-subsets regression. These best-ranked gain and loss models have weights of 0.310 and 0.132
1137 respectively, which is almost double the weight of the second ranked models (0.152 and 0.075
1138 respectively). In Supplementary Table 2 we also used the model.avg function of the MuMIn package
1139 to calculate a weighted mean of the coefficients of the best-ranked models together representing a

1140 cumulative weight-sum of 0.95 (i.e. a 95% confidence subset). Supplementary Table 2 (model-
1141 averaged) and main text Table 2 (best-ranked) model parameters are very similar. Supplementary
1142 Tables 3 and 4 report the complete sets of carbon gains and loss models that contribute to the model
1143 average results.

1144

1145 The model-average results show the same continental differences in sensitivity to environmental
1146 variables as the best-ranked models. From 2000 to 2015, carbon gains increased due to CO₂-change
1147 (+3.7% in both the averaged and the best-ranked models, both continents), while temperature rises led
1148 to a decline in gains, which especially had an effect in the Amazon (-1.14% and -1.07% due to MAT
1149 and MAT-change together in the averaged and best-ranked model respectively). Finally, both models
1150 result in similar predictions of the net carbon sink over the 1983-2040 period: the future net sink trend
1151 in Africa is -0.004 and -0.003 in the best-ranked and averaged models respectively; in Amazonia the
1152 future net sink trend is -0.013 and -0.011 in the best-ranked and averaged models respectively. The
1153 Amazon sink reaches zero in 2041 using model-averaged parameters compared to 2035 using the best-
1154 ranked models.

1155

1156 **Estimating Future Predictor Variables to 2040**

1157 To calculate future modelled trends in carbon gains and losses (Figure 3), we first estimated annual
1158 records of the predictor variables (CO₂-change, MAT, MAT-change, MCWD, WD and CRT) to 2040
1159 (Extended Data Figure 5).

1160

1161 To do so we first calculated annual records for the period of the observed trends for each plot location
1162 (i.e. from 1983-2014 in Africa and 1983-2011.5 in Amazonia). For CO₂-change, MAT, MAT-change
1163 and MCWD we extracted monthly records as described in section Predictor Variable Estimates
1164 (above). For WD and CRT we interpolated to a 0.1-yr period within each census interval (as in Figure

1165 1). Then, we calculated the mean annual value of each predictor variable from the 244 plot locations
1166 in Africa, and separately the mean annual value of each predictor variable from the 321 plot locations
1167 in Amazonia (i.e. solid lines in ED Figure 5). For each predictor variable, we calculated annual records
1168 of upper and lower confidence intervals by respectively adding and subtracting 2σ to the mean of each
1169 annual value (shaded area in ED Figure 5).

1170

1171 Secondly, for each predictor variable we parameterised a linear model for each continent using the
1172 annual records for the period of the observed trends. Then for each predictor variable, the continent-
1173 specific linear regression models were used to estimate predictor variables for each plot location from
1174 2014 to 2040 in Africa and from 2011.5 to 2040 in the Amazon (dotted lines in Extended Data Figure
1175 5). For each predictor variable, we calculated annual records of upper and lower confidence intervals
1176 by respectively adding and subtracting 2σ to the slope of each linear model (shaded area around dotted
1177 lines in ED Figure 5).

1178

1179 **Estimating Future Carbon Gain, Loss and Net Carbon Sink**

1180 We used the minimum adequate models (Table 2) to predict annual records of carbon gain, carbon loss
1181 and the carbon sink for the plot networks in Africa and Amazonia over the period 1983 through to
1182 2040 (Figure 3). We extracted fitted carbon gain and loss values using the mean annual records for
1183 each predictor variable (predictSE.lme function, AICcmodavg package¹⁰⁰). Upper and lower
1184 confidence intervals were calculated accounting for uncertainties in the model (both fixed and random
1185 effects) and predictor variables using the 2σ upper and lower confidence interval for each predictor
1186 variable (using predictSE.lme). Finally the net carbon sink was calculated by subtracting the losses
1187 from the gains. To obtain sink values in the future in Table 1, annual per unit area sink predictions,
1188 from Figure 3, were averaged over each decade and multiplied by the future forest area, as described
1189 above.

1190

1191 To test the sensitivity of the future predictions in Figure 3, we reran the analysis by modifying future
1192 trajectories of predictor variables one at a time, while keeping all others the same, to assess the mean
1193 C sink over 2010-15 and 2030 (averaging at 2030 is not necessary as trends in MAT-change and
1194 MCWD, which largely drive modelled inter-annual variability, are estimated as smooth trends in the
1195 future). For each predictor variable, we explored potential impacts of the likely bounds of possibility,
1196 (i) by taking the steepest slope of either continent from the extrapolated trends, doubling this slope and
1197 applying it on both continents; and (ii) by taking the steepest slope of either continent from the
1198 extrapolated trends, taking the opposite of this slope and applying it on both continents. These bounds
1199 represent deviations of >2 sigma from observed trends. Change in MAT also alters MAT-change, so
1200 we present the sensitivity of both parameters together.

1201

1202 Additionally, for CO₂-change and MAT, we also calculated future slopes under three future
1203 Representative Concentration Pathway (RCP) scenarios³⁸ with different radiative forcing in 2100:
1204 RCP2.6, 4.5, and 8.5. Future RCP CO₂-change slopes (ppm yr⁻¹) were calculated using RCP CO₂
1205 concentration data for the years between 2015 and 2030 inclusive. Future RCP MAT and MAT-change
1206 slopes were obtained from plot-specific MAT values extracted from downscaled 30 seconds resolution
1207 data for current⁸⁰ and future⁵¹ climate from WorldClim, and averaged over 19 CMIP5 models. We
1208 subtracted the mean 2040-2060 climate MAT (i.e. 2050) from the mean 1970-2000 climate MAT (i.e.
1209 1985), divided by 65 years to give the annual rate of change. We then calculated a mean slope over all
1210 plots per continent. Finally, to avoid mismatches between RCP-derived values of CO₂ and MAT and
1211 the observed records we removed any difference in intercept between the RCP trends and observed
1212 trends, so the RCP trends were a continuation of the end-point of the observed trajectory in 2015. We
1213 did not estimate the sensitivity of MCWD under the RCP scenarios, because the CMIP5 model means
1214 do not show drought trends for our forest plot networks, unlike rain gauge data for the recent past, and

1215 thus would show little or no sensitivity to MCWD. For each modified slope, Supplementary Table 5
1216 reports the absolute decline in the sink in each continent in 2030 compared to the 2010-15 mean sink.
1217 This shows that the future sink strength is sensitive to future environmental conditions, but within both
1218 RCP scenarios and our bounds of possibility we show a decline in the sink strength in both continents
1219 over the 2020s.

1220

1221 **Data and Code Availability**

1222 Source data and R-code to generate figures and tables are available from:
1223 http://dx.doi.org/10.5521/Forestplots.net/2019_1

1224

1225 **References (Methods only)**

- 1226 51 Hijmans, R. J., Cameron, S. E., Parra, J. L., Jones, P. G. & Jarvis, A. Very high resolution
1227 interpolated climate surfaces for global land areas. *International Journal of Climatology* **25**,
1228 1965-1978, doi:10.1002/joc.1276 (2005).
- 1229 52 Lopez-Gonzalez, G., Lewis, S. L., Burkitt, M. & Phillips, O. L. ForestPlots.net: a web
1230 application and research tool to manage and analyse tropical forest plot data. *Journal of*
1231 *Vegetation Science* **22**, 610–613, doi:10.1111/j.1654-1103.2011.01312.x (2011).
- 1232 53 Lopez-Gonzalez, G., Lewis, S. L., Burkitt, M., T.R., B. & Phillips, O. L. ForestPlots.net
1233 Database. www.forestplots.net. Date of extraction [10/11/2017]. (2009).
- 1234 54 Sheil, D. & Bitariho, R. Bwindi Impenetrable Forest TEAM Site. Data Set Identifier: TEAM-
1235 DataPackage-20151201235855_1254. (2009).
- 1236 55 Kenfack, D. Korup National Park TEAM Site. Data Set Identifier: TEAM-DataPackage-
1237 20151201235855_1254. (2011).
- 1238 56 Rovero, F., Marshall, A. & Martin, E. Udzungwa TEAM Site. Data Set Identifier: TEAM-
1239 DataPackage-20151130235007_5069. (2009).

- 1240 57 Hockemba, M. B. N. Nouabalé Ndoki TEAM Site. Data Set Identifier: TEAM-DataPackage-
1241 20151201235855_1254. (2010).
- 1242 58 Anderson-Teixeira, K. J. *et al.* CTFS-ForestGEO: a worldwide network monitoring forests in
1243 an era of global change. *Global Change Biology* **21**, 528-549, doi:10.1111/gcb.12712 (2015).
- 1244 59 Gourlet-Fleury, S. *et al.* Tropical forest recovery from logging: a 24 year silvicultural
1245 experiment from Central Africa. *Philosophical Transactions of the Royal Society B-Biological*
1246 *Sciences* **368**, 20120302, doi:10.1098/rstb.2012.0302 (2013).
- 1247 60 Claeys, F. *et al.* Climate change would lead to a sharp acceleration of Central African forests
1248 dynamics by the end of the century. *Environmental Research Letters* **14**, 044002,
1249 doi:10.1088/1748-9326/aafb81 (2019).
- 1250 61 Chave, J. *et al.* Improved allometric models to estimate the aboveground biomass of tropical
1251 trees. *Global Change Biology* **20**, 3177-3190, doi:10.1111/gcb.12629 (2014).
- 1252 62 R Development Core Team. R: A Language and Environment for Statistical Computing.
1253 Available at <http://www.R-project.org/>. (2015).
- 1254 63 Lopez-Gonzalez, G., Sullivan, M. & Baker, T. BiomasaFP package. Tools for analysing data
1255 downloaded from ForestPlots.net. R package version 0.2.1. Available at
1256 <http://www.forestplots.net/en/resources/analysis>. (2017).
- 1257 64 Phillips, O., Baker, T., Brien, R. & Feldpausch, T. RAINFOR field manual for plot
1258 establishment and remeasurement. Available at
1259 http://www.rainfor.org/upload/ManualsEnglish/RAINFOR_field_manual_version_2016.pdf.
1260 (2016).
- 1261 65 Talbot, J. *et al.* Methods to estimate aboveground wood productivity from long-term forest
1262 inventory plots. *Forest Ecology and Management* **320**, 30-38,
1263 doi:10.1016/j.foreco.2014.02.021 (2014).

- 1264 66 Sullivan, M. J. P. *et al.* Field methods for sampling tree height for tropical forest biomass
1265 estimation. *Methods in Ecology and Evolution* **9**, 1179-1189, doi:10.1111/2041-210X.12962
1266 (2018).
- 1267 67 Feldpausch, T. R. *et al.* Tree height integrated into pantropical forest biomass estimates.
1268 *Biogeosciences* **9**, 3381-3403, doi:10.5194/bg-9-3381-2012 (2012).
- 1269 68 Chave, J. *et al.* Towards a worldwide wood economics spectrum. *Ecology Letters* **12**, 351-366,
1270 doi:10.1111/j.1461-0248.2009.01285.x (2009).
- 1271 69 Zanne, A. E. *et al.* *Data from: Towards a worldwide wood economics spectrum* (Dryad Digital
1272 Repository, 2009).
- 1273 70 Martin, A. R., Doraisami, M. & Thomas, S. C. Global patterns in wood carbon concentration
1274 across the world's trees and forests. *Nature Geoscience* **11**, 915-920, doi:10.1038/s41561-018-
1275 0246-x (2018).
- 1276 71 Kohyama, T. S., Kohyama, T. I., Sheil, D. & Rees, M. Definition and estimation of vital rates
1277 from repeated censuses: Choices, comparisons and bias corrections focusing on trees. *Methods*
1278 *in Ecology and Evolution* **9**, 809-821, doi:10.1111/2041-210x.12929 (2018).
- 1279 72 Bates, D., Maechler, M., Bolker, B. & Walker, S. lme4: Linear mixed-effects models using
1280 Eigen andS4.Rpackage version, 1.0-4. Available at [http://www.inside-](http://www.inside-r.org/packages/lme4/versions/1-0-4)
1281 [r.org/packages/lme4/versions/1-0-4](http://www.inside-r.org/packages/lme4/versions/1-0-4). (2013).
- 1282 73 Fox, J. *Applied Regression Analysis and Generalized Linear Models*. Second edn, (Sage
1283 Publishing, 2008).
- 1284 74 Chave, J. *et al.* Assessing evidence for a pervasive alteration in tropical tree communities. *PLoS*
1285 *Biology* **6**, 0455-0462, doi:10.1371/journal.pbio.0060045 (2008).
- 1286 75 Yuen, J. Q., Ziegler, A. D., Webb, E. L. & Ryan, C. M. Uncertainty in below-ground carbon
1287 biomass for major land covers in Southeast Asia. *Forest Ecology and Management* **310**, 915-
1288 926, doi:10.1016/j.foreco.2013.09.042 (2013).

- 1289 76 Aragão, L. E. O. C. *et al.* Spatial patterns and fire response of recent Amazonian droughts.
1290 *Geophysical Research Letters* **34**, 1-5, doi:10.1029/2006gl028946 (2007).
- 1291 77 Aragão, L. E. O. C. *et al.* Environmental change and the carbon balance of Amazonian forests.
1292 *Biological Reviews* **89**, 913-931, doi:10.1111/brv.12088 (2014).
- 1293 78 Tans, P. & Keeling, R. Mauna Loa CO₂ monthly mean data. Available at
1294 <http://www.esrl.noaa.gov/gmd/ccgg/trends/>. (2016).
- 1295 79 Harris, I., Jones, P. D., Osborn, T. J. & Lister, D. H. Updated high-resolution grids of monthly
1296 climatic observations – the CRU TS3.10 Dataset. *International Journal of Climatology* **34**,
1297 623–642 doi:10.1002/joc.3711 (2014).
- 1298 80 Fick, S. E. & Hijmans, R. J. WorldClim 2: new 1-km spatial resolution climate surfaces for
1299 global land areas. *International Journal of Climatology* **37**, 4302-4315, doi:10.1002/joc.5086
1300 (2017).
- 1301 81 Ramirez-Villegas, J. & Jarvis, A. Downscaling Global Circulation Model Outputs: The Delta
1302 Method. Decision and Policy Analysis Working Paper No. 1., 18 (2010).
- 1303 82 Schneider, U. *et al.* GPCP Full Data Reanalysis Version 6.0 at 0.5°: Monthly Land-Surface
1304 Precipitation from Rain-Gauges built on GTS-based and Historic Data.
1305 doi:10.5676/DWD_GPCP/FD_M_V6_050 (2011).
- 1306 83 Sun, Q. *et al.* Review of Global Precipitation Data Sets: Data Sources, Estimation, and
1307 Intercomparisons. *Reviews of geophysics* **56**, 79-107, doi:10.1002/ (2017).
- 1308 84 Huffman, G. J. *et al.* The TRMM Multisatellite Precipitation Analysis (TMPA): Quasi-Global,
1309 Multiyear, Combined-Sensor Precipitation Estimates at Fine Scales. *Journal of*
1310 *Hydrometeorology* **8**, 38-55, doi:10.1175/jhm560.1 (2007).
- 1311 85 Kume, T. *et al.* Ten-year evapotranspiration estimates in a Bornean tropical rainforest.
1312 *Agricultural and Forest Meteorology* **151**, 1183-1192, doi:10.1016/j.agrformet.2011.04.005
1313 (2011).

- 1314 86 Zelazowski, P., Malhi, Y., Huntingford, C., Sitch, S. & Fisher, J. B. Changes in the potential
1315 distribution of humid tropical forests on a warmer planet. *Philosophical Transactions of the*
1316 *Royal Society A: Mathematical, Physical and Engineering Sciences* **369**, 137-160,
1317 doi:10.1098/rsta.2010.0238 (2011).
- 1318 87 James, R., Washington, R. & Rowell, D. P. Implications of global warming for the climate of
1319 African rainforests. *Philosophical transactions of the Royal Society of London. Series B,*
1320 *Biological sciences* **368**, 20120298, doi:10.1098/rstb.2012.0298 (2013).
- 1321 88 Jung, M. *et al.* Recent decline in the global land evapotranspiration trend due to limited
1322 moisture supply. *Nature* **467**, 951-954, doi:10.1038/nature09396 (2010).
- 1323 89 Jung, M. *et al.* Global patterns of land-atmosphere fluxes of carbon dioxide, latent heat, and
1324 sensible heat derived from eddy covariance, satellite, and meteorological observations. *Journal*
1325 *of Geophysical Research* **116**, doi:10.1029/2010jg001566 (2011).
- 1326 90 Lloyd, J. & Farquhar, G. D. The CO₂ dependence of photosynthesis, plant growth responses to
1327 elevated atmospheric CO₂ concentrations and their interaction with soil nutrient status. I.
1328 General principles and forest ecosystems. *Functional Ecology* **10**, 4-32, doi:10.2307/2390258
1329 (1996).
- 1330 91 Aspinwall, M. J. *et al.* Convergent acclimation of leaf photosynthesis and respiration to
1331 prevailing ambient temperatures under current and warmer climates in *Eucalyptus tereticornis*.
1332 *New Phytol* **212**, 354-367, doi:10.1111/nph.14035 (2016).
- 1333 92 Bonal, D., Burban, B., Stahl, C., Wagner, F. & Hérault, B. The response of tropical rainforests
1334 to drought—lessons from recent research and future prospects. *Annals of Forest Science* **73**,
1335 27-44, doi:10.1007/s13595-015-0522-5 (2016).
- 1336 93 Quesada, C. A. *et al.* Variations in chemical and physical properties of Amazon forest soils in
1337 relation to their genesis. *Biogeosciences* **7**, 1515-1541, doi:10.5194/bg-7-1515-2010 (2010).

- 1338 94 Baker, T. R., Swaine, M.D., Burslem, D.F.R.P. Variation in tropical forest growth rates:
1339 combined effects of functional group composition and resource availability. *Perspectives in*
1340 *Plant Ecology, Evolution and Systematics* **6**, 21-36, doi:10.1078/1433-8319-00040 (2003).
- 1341 95 Pinheiro, J. C. & Bates, D. M. *Mixed-Effects Models in S and S-PLUS*. First edn, 528 (Springer,
1342 2000).
- 1343 96 Venables, W. N. & Ripley, B. D. *Modern Applied Statistics with S*. Fourth edn, 498 (Springer,
1344 2002).
- 1345 97 Olejnik, S., Mills, J. & Keselman, H. Using Wherry's Adjusted R^2 and Mallows' Cp for Model
1346 Selection From All Possible Regressions. *The Journal of Experimental Education* **68**, 365-380,
1347 doi:10.1080/00220970009600643 (2000).
- 1348 98 Whittingham, M. J., Stephens, P. A., Bradbury, R. B. & Freckleton, R. P. Why do we still use
1349 stepwise modelling in ecology and behaviour? *Journal of Animal Ecology* **75**, 1182-1189,
1350 doi:10.1111/j.1365-2656.2006.01141.x (2006).
- 1351 99 Bartoń, K. MuMIn: Multi-Model Inference. Tools for performing model selection and model
1352 averaging. R package version 1.43.6. (2019).
- 1353 100 Gelman, A. & Hill, J. *Data Analysis Using Regression and Multilevel/Hierarchical Models*.
1354 (Cambridge University Press, New York, 2007).
- 1355 101 Mayaux, P., De Grandi, G. & Malingreau, J.-P. Central African Forest Cover Revisited: A
1356 Multisatellite Analysis. *Remote Sensing of Environment* **71**, 183–196, doi:10.1016/S0034-
1357 4257(99)00073-5 (2000).

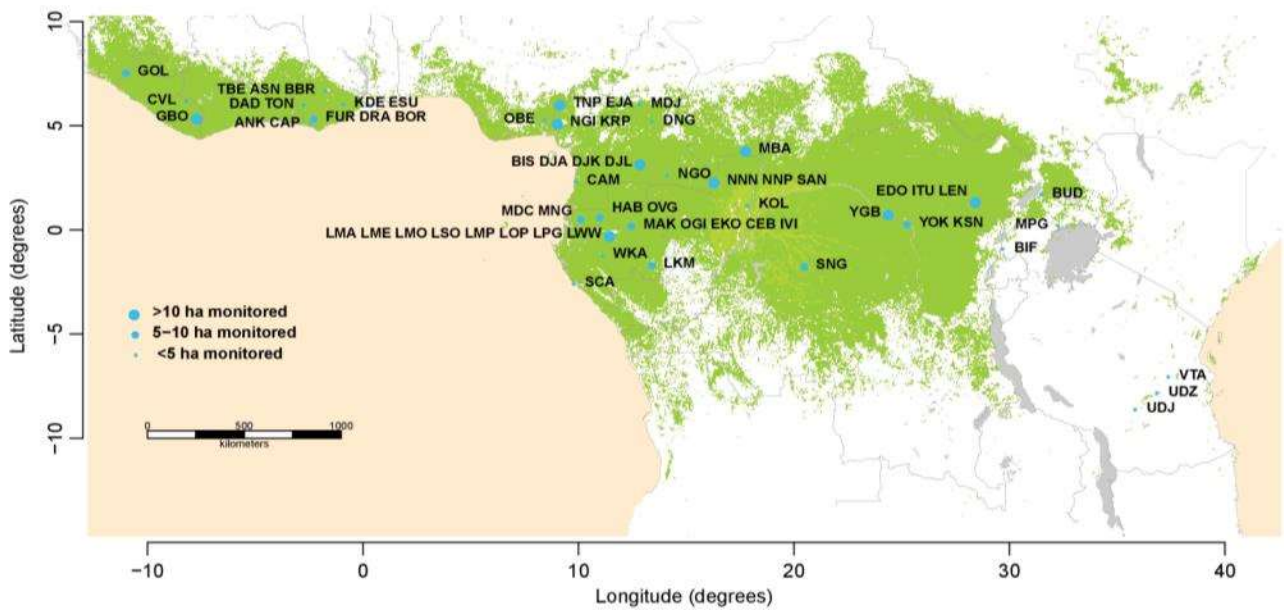
1358

1359 **Author Information**

1360 Correspondence and requests for materials should be addressed to W.H. (whubau@gmail.com). The
1361 authors declare no competing financial interests. Supplementary Information is available online for
1362 this paper.

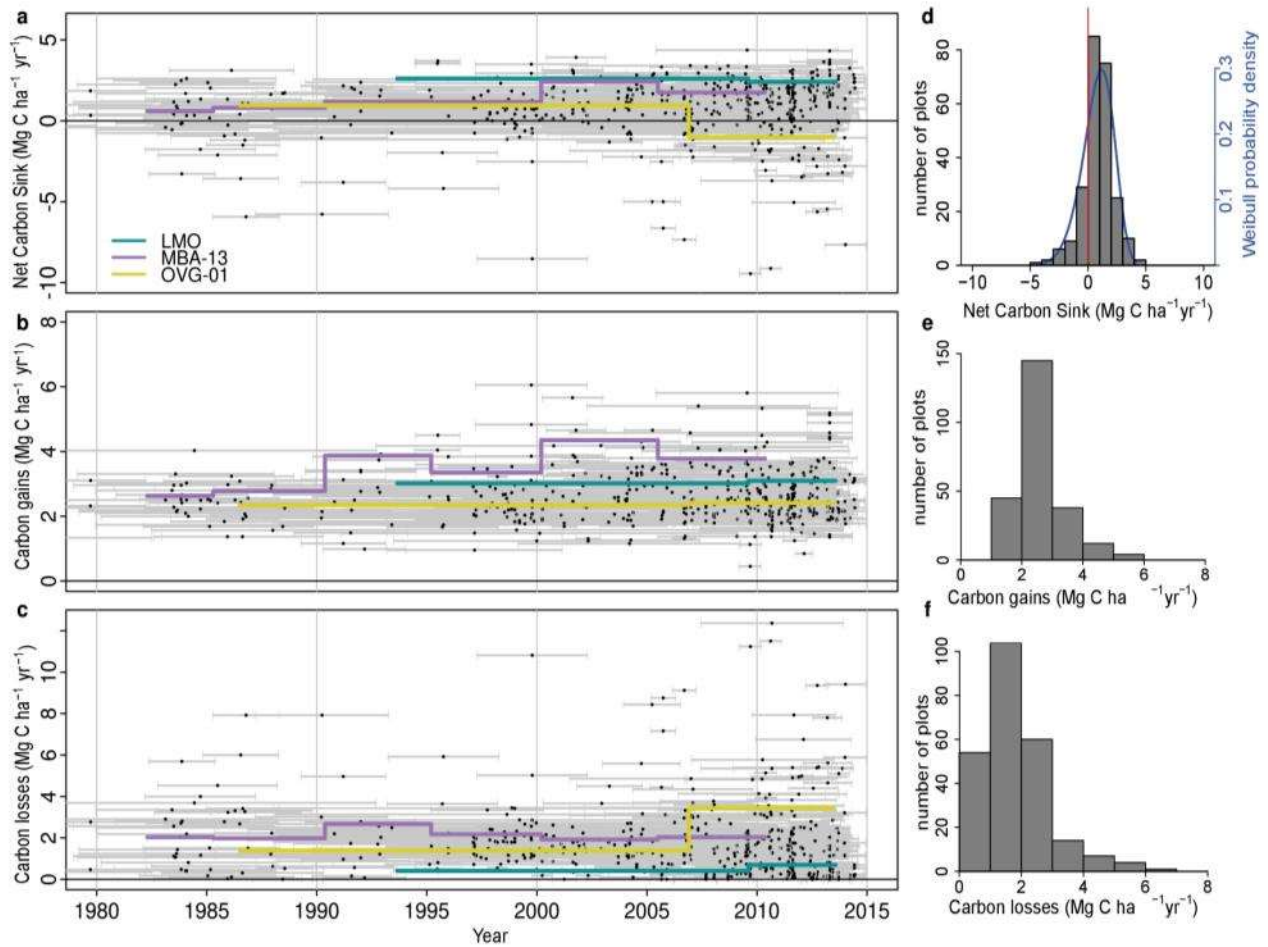
1363

1364 **Extended Data Figures**



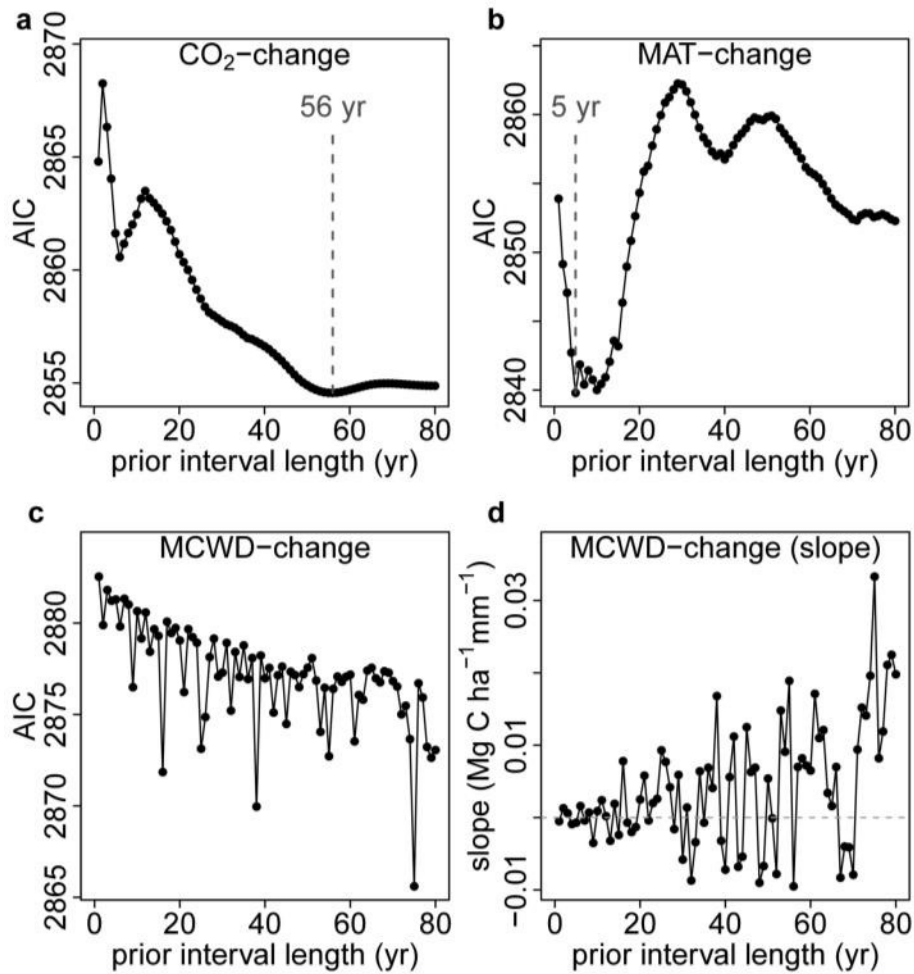
1365

1366 **Extended Data Figure 1. Map showing the locations of the 244 plots included in this study.** Dark
1367 green represents all lowland closed-canopy forests, submontane forests and forest-agriculture mosaics;
1368 light green shows swamp forests and mangroves¹⁰¹, blue circles represent plot clusters, referred to by
1369 three-letter codes (see Supplementary Table 1 for the full list of plots). Clusters <50 km apart are
1370 shown as one point for display only, with the circlesize corresponding to sampling effort in terms of
1371 hectares monitored.



1372

1373 **Extended Data Figure 2. Long-term above-ground carbon dynamics of 244 African intact**
 1374 **tropical forest inventory plots.** Points in the scatterplots indicate the mid-census interval date, with
 1375 horizontal bars connecting the start and end date for each census interval for net aboveground biomass
 1376 carbon change (a), carbon gains (from woody production from tree growth and newly recruited stems)
 1377 (b), and carbon losses (from tree mortality) (c). Examples of time series for three individual plots are
 1378 shown in purple, yellow and green. Associated histograms show the distribution of the plot-level net
 1379 aboveground biomass carbon (d) (with a three-parameter Weibull probability density distribution fitted
 1380 in blue, showing the carbon sink is significantly larger than zero; one-tail t-test: $p < 0.001$), carbon gains
 1381 (e), and carbon losses (f).

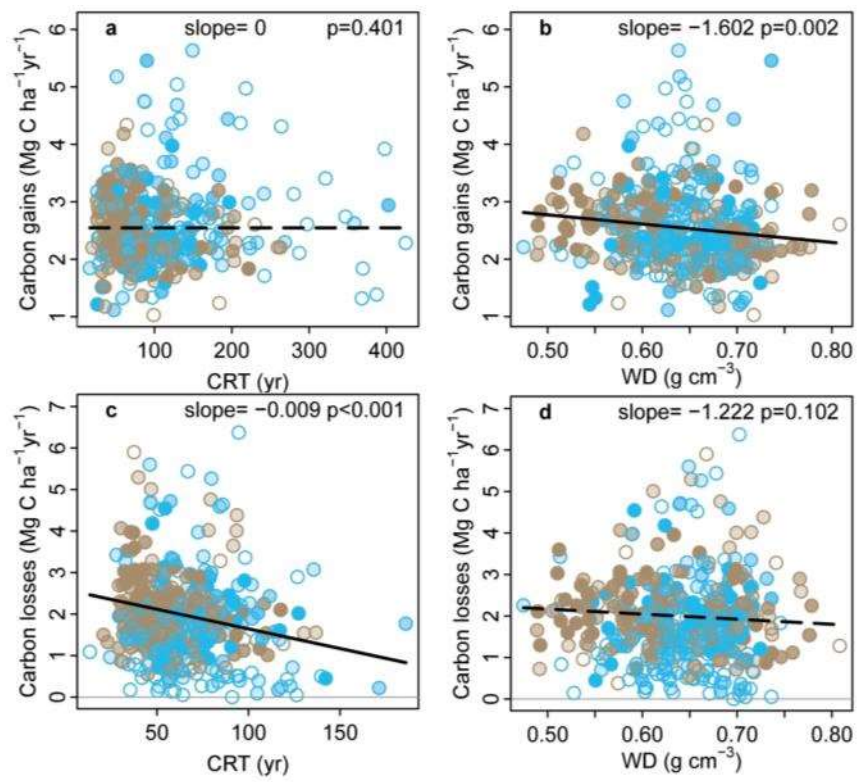


1382

1383 **Extended Data Figure 3. Akaike's Information Criterion (AIC) from correlations between the**
 1384 **carbon gain in tropical forest inventory plots and changes in either atmospheric CO₂,**
 1385 **temperature (as MAT) or drought (as MCWD), each calculated over ever-longer prior intervals.**
 1386 Panels show AIC from linear mixed effects models of carbon gains from 565 plots and corresponding,
 1387 atmospheric CO₂ (CO₂-change) (a), Mean Annual Temperature (MAT-change) (b), and Maximum
 1388 Climatological Water Deficit (MCWD-change) (c). For CO₂ the AIC minimum was observed when
 1389 predicting the carbon gain from the change in CO₂ calculated over a 56 year long prior interval length.
 1390 We use this length of time to calculate our CO₂-change parameter. Such a value is expected because
 1391 forest stands will respond most strongly to CO₂ when most individuals have grown under the new
 1392 rapidly changing condition, which should be at its maximum at a time approximately equivalent to the
 1393 carbon residence time of a forest stand^{30,90} (mean of 62 years in this pooled African and Amazonian

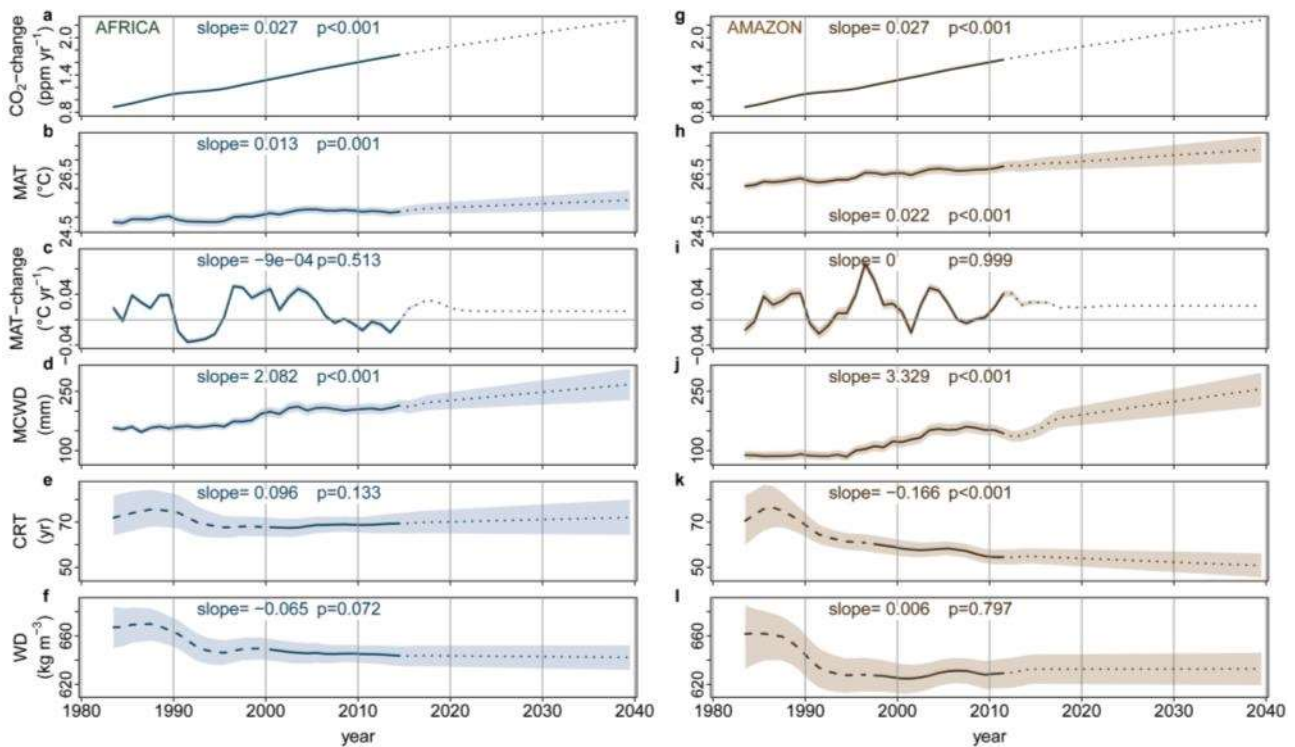
1394 dataset). For MAT the AIC minimum was 5 years, which we use as the prior interval to calculate our
 1395 MAT-change parameter. This length is consistent with experiments showing temperature acclimation
 1396 of leaf- and plant-level photosynthetic and respiration processes over approximately half-decadal
 1397 timescales^{31,91}. For MCWD the AIC minimum is not obvious, while the slope of the correlation, shown
 1398 in panel (d), shows no overall trend and oscillates between positive or negative values, meaning there
 1399 is no relationship between carbon gains and the change in MCWD over intervals longer than 1 year;
 1400 thus MCWD-change is not included in our models. This result suggests that once a drought ends, its
 1401 impact on tree growth fades rapidly, as seen in other studies^{14,92}. Also in the moist tropics wet-season
 1402 rainfall is expected to re-charge soil water, hence lagged impacts of droughts are not expected.

1403
 1404
 1405
 1406
 1407



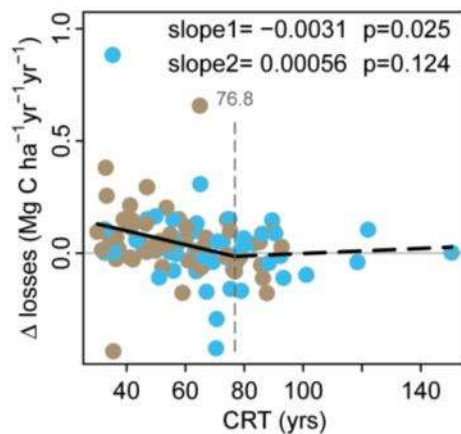
1408

1409 **Extended Data Figure 4. Potential forest dynamics-related drivers of carbon gains and losses in**
 1410 **structurally intact African and Amazonian tropical forest inventory plots.** The aboveground
 1411 carbon gains, from woody production (**a-b**), and aboveground carbon losses, from tree mortality (**c-**
 1412 **d**), are plotted against the carbon residence time (CRT), and wood density (WD), for African (blue)
 1413 and Amazonian (brown) inventory plots. Linear mixed effect models were performed with census
 1414 intervals ($n=1566$) nested within plots ($n=565$) to avoid pseudo-replication, using an empirically
 1415 derived weighting based on interval length and plot area (see methods). Significant regression lines
 1416 for the complete dataset are shown as a solid line; non-significant regressions as a dashed line. Each
 1417 dot represents a time-weighted mean plot-level value; transparency of the inner part of the dot
 1418 represents total monitoring length, with empty circles corresponding to plots monitored for ≤ 5 years
 1419 and solid circles for plots monitored for >20 years. Carbon loss data are presented untransformed for
 1420 comparison with carbon gains; linear mixed effects models on transformed data to fit normality
 1421 assumptions do not change the significance of the results. Note, CRT is calculated differently for the
 1422 carbon gains and losses models (see methods).



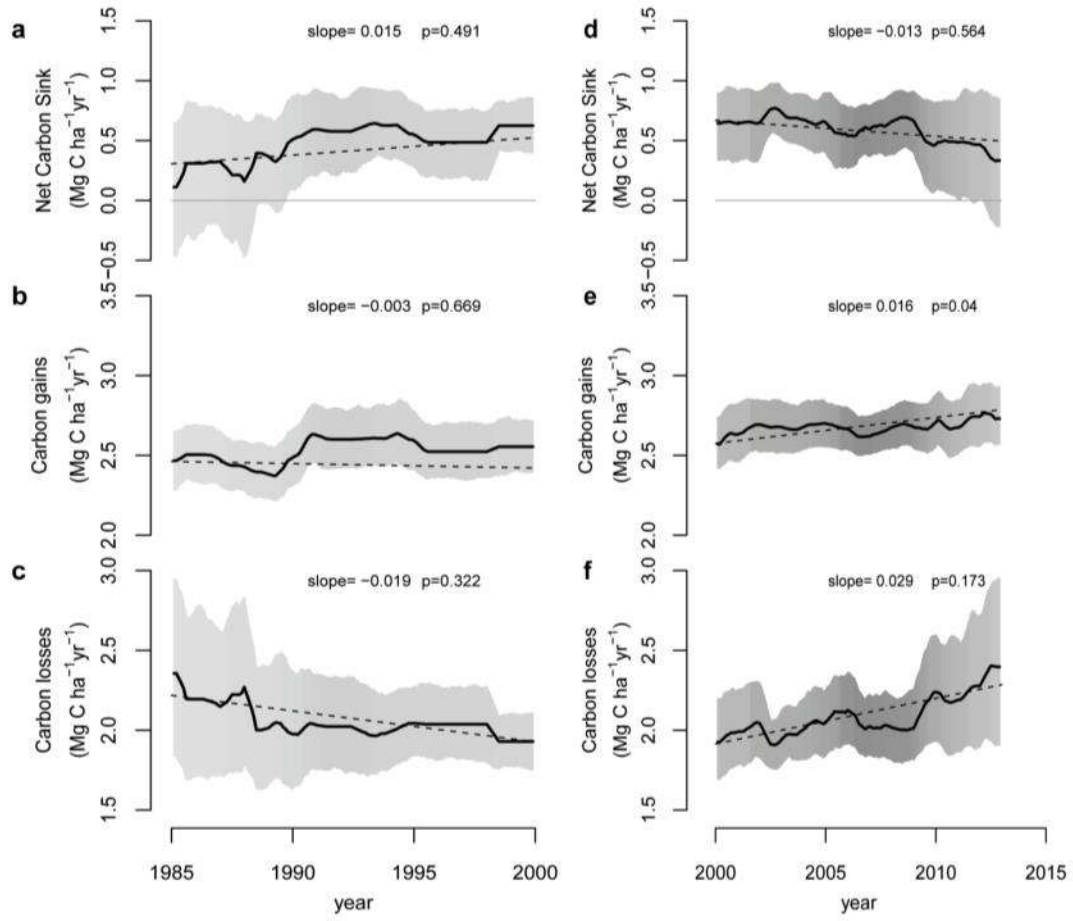
1423

1424 **Extended Data Figure 5. Trends in predictor variables used to estimate long-term trends in**
 1425 **above-ground carbon gains, carbon losses and the resulting net carbon sink in African and**
 1426 **Amazonian intact tropical forest plot networks.** Mean annual CO₂-change (a), MAT (b), MAT-
 1427 change (c), MCWD (d), CRT (e), and WD (f) for African plot locations in blue, and corresponding
 1428 Amazon plots locations in brown (g-i). Solid lines for CO₂-change, MAT, MAT-change, MCWD
 1429 represent observational data, and solid lines for CRT and WD represent plot means and a time window
 1430 where >75% of the plots were monitored, long-dashed lines are plot means were <75% of plots were
 1431 monitored. Dotted lines are future values estimated from linear trends on the 1983-2014 (Africa) or
 1432 1983-2011 (Amazon) data (slope and p-value reported in each panel), see methods for details. Upper
 1433 and lower confidence intervals (shaded area) for the past (Africa: 1983-2014; Amazonia: 1983-2011)
 1434 are calculated by respectively adding and subtracting 2σ to the mean of each annual value. Upper and
 1435 lower confidence intervals for the future were estimated by adding and subtracting 2σ from the slope
 1436 of the regression model.



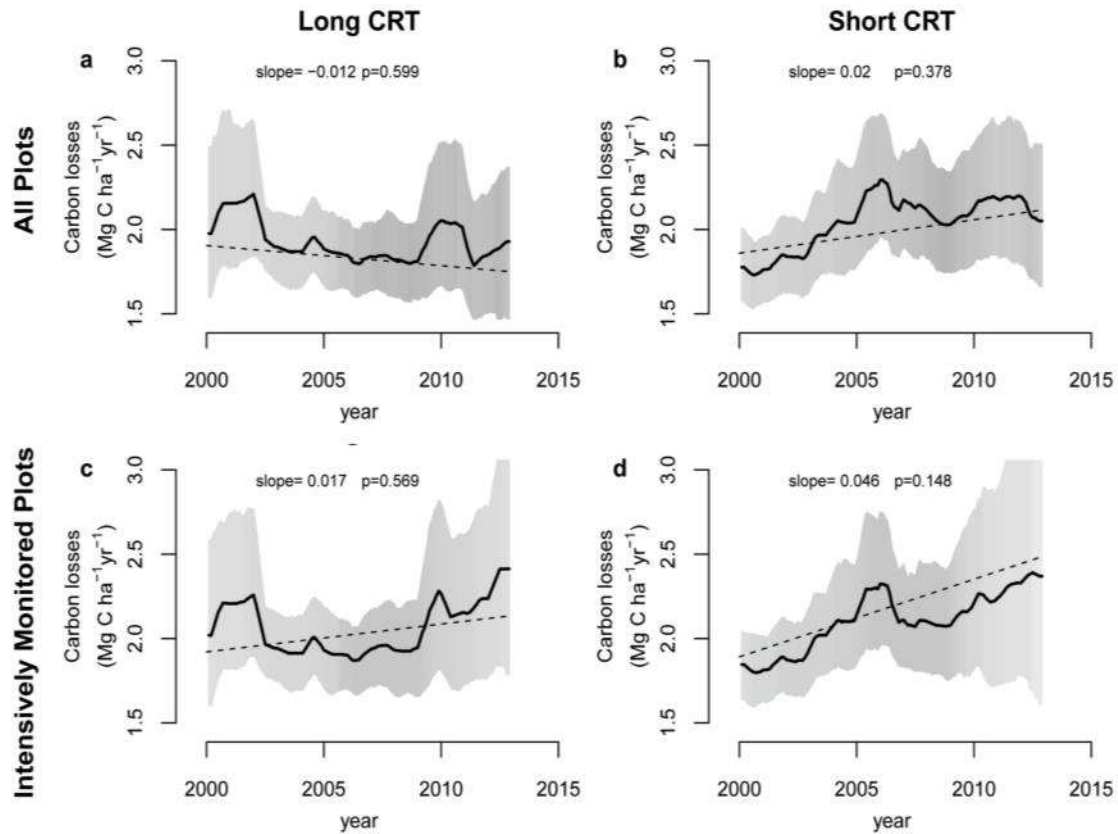
1437
 1438 **Extended Data Figure 6. The change in carbon losses versus carbon residence time (CRT) of**
 1439 **inventory plots in Africa and Amazonia.** For plots with two census intervals, we calculated the
 1440 change in carbon losses (Δ losses, in Mg C ha⁻¹ yr⁻¹ yr⁻¹) as the carbon losses (Mg C ha⁻¹ yr⁻¹) of the
 1441 second interval minus the carbon losses of the first interval, divided by the difference in mid-interval
 1442 dates. For plots with more than two intervals, we calculated the change in carbon losses for each pair
 1443 of subsequent intervals, then calculated the plot-level mean over all pairs, weighted by the time length

1444 between mid-interval dates. This analysis includes only plots with at least two census intervals and
 1445 monitored for ≥ 20 years (i.e. roughly one-third of the mean CRT of the pooled African and Amazon
 1446 dataset; $n = 116$). Breakpoint regression was used to assess the CRT length below which forest carbon
 1447 losses begin to increase. Plots with CRT < 77 years show a recent long-term increase in carbon losses,
 1448 longer CRT plots do not. Blue points are African plots, brown points are Amazonian plots.



1449
 1450 **Extended Data Figure 7. Trends in African tropical forest net aboveground live biomass carbon,**
 1451 **carbon gains and carbon losses, calculated for the last 15 years of the twentieth century (left**
 1452 **panels a-c) and the first 15 years of the twenty-first century (right panels d-f).** Plots were selected
 1453 from the full dataset if their census intervals cover at least 50% of the respective time windows, i.e.
 1454 they are intensely monitored ($n=56$ plots for 1985-2000, and $n=134$ plots for 2000-2015, respectively).
 1455 Solid lines show mean values, shading corresponds to the 95% CI, as calculated in Figure 1. Dashed
 1456 lines, slopes and p-values are from linear mixed effects models, as in Figure 1. The data shows a

1457 difference compared to Figure 1, notably the sink decline after ~2010 driven by rising carbon losses.
 1458 This is because in Figure 1 we include all available plots over the 1983-2015 window, which includes
 1459 clusters of plots monitored *only* in the 2010s that had low carbon loss and high carbon sink values.



1460
 1461 **Extended Data Figure 8. Twenty-first century trends in aboveground biomass carbon losses**
 1462 **from African tropical forest inventory plots with either long (left panels) or short (right panels)**
 1463 **carbon residence time.** Upper panels include all plots, i.e. as in Figure 1, but split into a long-CRT
 1464 group (a), and a short-CRT group (b), each containing half the 244 plots. Lower panels restrict plots
 1465 to those spanning >50% of the time window, i.e. intensely monitored plots, as in Extended Data Figure
 1466 7, but split into a long-CRT group (c), and a short-CRT group (d), each containing half the 134 plots.
 1467 Solid lines indicate mean values, shading the 95% CI, as for Figure 1. Dashed lines, slopes and p-
 1468 values are from linear mixed-effects models, as for Figure 1. Carbon losses increase at a higher rate in
 1469 the short-CRT than the long-CRT group of plots, in both datasets, although this increase is not
 1470 statistically significant.

1471

1472

1473

1474 **Extended Data Tables**

1475

1476 **Extended Data Table 1.** Models to predict carbon gains and losses in African and Amazonian tropical
 1477 forests, including only environmental variables, showing long-term trends that impact theory-driven
 1478 models of photosynthesis and respiration. Significant values in bold.

Carbon gains, Mg C ha ⁻¹ yr ⁻¹				
Predictor variable	Parameter value	Standard Error	t-value	p-value
(Intercept)	4.694	0.739	6.354	0.000
CO ₂ (ppm)	0.005	0.001	3.196	0.001
MAT (°C)	-0.143	0.021	-6.844	0.000
MCWD (mm x1000)	-1.232	0.210	-5.878	0.000
Carbon losses, Mg C ha ⁻¹ yr ⁻¹ *				
Predictor variable	Parameter value	Standard Error	t-value	p-value
(Intercept)	0.926	1.854	0.500	0.617
CO ₂ (ppm)	0.004	0.004	0.947	0.344
MAT (°C)	-0.011	0.044	-0.249	0.804
MCWD (mm x1000)	-0.498	0.505	-0.985	0.325

1479

* carbon loss values were normalized via power-law transformation, $\lambda = 0.361$.

1480

1481 **Extended Data Table 2.** Forest area estimates used to calculate total continental forest sink.

Period	intact forest area (Mha)*			
	Africa	Amazon	Southeast Asia	Pan-tropics
1980	671.5	958.3	233.6	1863.4
1985	634.3	921.1	207.4	1762.8
1990	600.2	885.2	190.6	1676.0
1995	565.9	851.1	163.5	1580.5
2000	531.8	817.2	136.9	1485.9
2005	504.8	784.5	129.2	1418.5
2010	477.8	756.3	118.4	1352.5
2015	450.5	726.7	101.5	1278.7
2020	425.5	698.5	90.1	1214.2
2025	402.0	671.5	80.0	1153.4
2030	379.7	645.4	71.0	1096.1
2035	358.6	620.4	63.0	1042.1
2040	338.8	596.4	56.0	991.1

* Intact forest area for 1990, 2000 and 2007 is published in ref. 1 (i.e. the total forest area minus forest regrowth). To estimate intact forest area for the other years in this table, we fitted exponential models for each continent using the published data.